Islamic University Journal of Applied Sciences (IUJAS)
https://journals.iu.edu.sa/jesc

Volume VIII, Issue II, December 2026, Pages 281-325

Recent Advances in Conformational Analysis and Spectral techniques, Compiled with Quantum Mechanical Calculations for Some Compounds

Usama. A. Soliman [1] *

[1] Chemistry Division, Department of Physical Sciences, College of Science, Jazan University, P.O. Box. 114, Jazan, 45142, Kingdom of Saudi Arabia.

*Corresponding author: (Usama A. Soliman) , *Email Address*: usoliman@jazanu.edu.sa

Abstract

Currently, quantum mechanical (QM) calculations are essential to support diverse chemical investigations by predicting electronic structures, reaction energies, and spectroscopic properties. Precise analysis of molecular conformations enables a comprehensive understanding of the structural, physicochemical properties of molecular systems. This decade has witnessed significant advancements in computational chemistry and spectroscopic techniques that have revolutionized conformational analysis, providing more accurate structural elucidation. Combination of QM calculations with experimental spectrum data (IR, NMR, UV-Vis, and Raman) has markedly improved the precision of conformational analysis and interpretation of spectral data. This review highlights significant advancements in conformational analysis, spectroscopic techniques, and their synergistic application with QM calculations, particularly density functional theory (DFT). The review presents case studies of chemically and biologically relevant molecules to illustrate the effectiveness of integrating experimental spectra and computational methods for conformational analysis and structural elucidation. This review also highlights the current limitations and proposes suggestions for future methodological improvements.

Keywords: Conformational analysis; Quantum mechanical calculations; IR/Raman; NMR; UV-Vis spectra.

https://doi.org/10.63070/jesc.2026.044
Received 20 May 2026; Revised 10 October 2026; Accepted 18 October 2026;
Available online 25 October 2026.
Published by Islamic University of Madinah on behalf of *Islamic University Journal of Applied Sciences.*
This is an open access article published under the Creative Commons Attribution 4.0 International license (CC BY 4.0): https://creativecommons.org/licenses/by/4.0/

1. Introduction

Conformational analysis and spectroscopy are essential tools for understanding the structures and properties of organic/inorganic compounds, pharmaceuticals, biomolecules, natural products, and polymers. These approaches enable researchers to ascertain the three-dimensional arrangement of atoms inside a molecule, which is essential for predicting physical, chemical, and biological aspects. Recent advances in computational chemistry, machine learning, and spectroscopic techniques have considerably improved the precision and efficacy of conformational analysis. The determination of molecular structure and conformational dynamics is a cornerstone of modern chemistry, with applications in drug design [1-3], catalysis [4, 5], and materials science [6-8].

X-ray crystallography and spectroscopic techniques (NMR, IR, Raman, UV-Vis, and MS) are the primary experimental methods for investigating molecular structure and conformations [9, 10]; however, they possess limitations. For example, X-ray crystallography requires high-quality single crystals, which may be difficult or impossible to obtain for several substances, including flexible molecules, amorphous materials, or proteins with low solubility [11]. Also, the accurate interpretation of the experimental vibrational and NMR spectra may be challenging, particularly for complex materials such as biomolecules and polymers, owing to band/signal overlap and the experimental conditions affecting the spectra [12, 13]. To overcome these challenges, quantum mechanical (QM) methods, particularly density functional theory (DFT), have become indispensable for predicting molecular conformations and their spectroscopic signatures [14]. NMR spectroscopy can distinguish between conformers, but it requires chemical shifts calculated by quantum mechanics to provide precise structural assignments [15]. Interpretation of complex peak patterns in IR and Raman spectra requires DFT-based vibrational frequency calculations [16]. UV-Vis and circular dichroism (CD) spectra are frequently analyzed by time-dependent (TD) DFT calculations to associate electronic transitions with molecular structure [17]. Computational chemistry involves the use of computer software to predict the electronic structure of a chemical species (atom, molecule, ion, or crystal) and its properties based on the concepts of quantum mechanics, molecular mechanics (MM), and molecular dynamics (MD) simulations [18]. This field of chemistry has diverse applications, including drug development, material science, and environmental chemistry, focusing on the prediction of molecular structures, energetics, and spectroscopic behavior [19]. Recent developments in computational chemistry allow for precise predictions of conformations and molecular properties, such as vibrational frequencies (IR/Raman), electronic transitions (UV-Vis), and NMR chemical shifts, which enable direct comparison with experimental data [17].

QM methods, such as DFT and *ab initio* calculations, can predict geometries without requiring crystallization, thereby allowing for structural investigations of amorphous or non-crystalline

compounds. Also, MD simulations effectively model flexible systems in solution [20], providing a connection between solid-state (X-ray) and solution (NMR) structures. DFT frequency calculations and normal coordinate analysis enable accurate assignment of vibrational modes to their respective observed IR/Raman bands, which are significant in distinguishing conformers based on their fingerprint regions [21, 22]. DFT-based NMR chemical shift calculations have clarified ambiguities in the conformational preferences of flexible organic molecules [23]. TD-DFT calculations of electronic circular dichroism (ECD) spectrum aid in the determination of absolute stereochemistry [24].

Despite the advancements in QM calculations, challenges persist, including the accurate modeling of weak interactions (such as dispersion forces and hydrogen bonding) and large, flexible systems. Recent advancements in machine learning-augmented quantum mechanics methods, improved sampling algorithms, and hybrid QM/MM approaches are advancing the field of conformational analysis. The integration of experimental spectral data with QM calculations has demonstrated significant efficacy, enabling researchers to validate theoretical models and refine conformational predictions [25]. This synergy has become indispensable, with particularly transformative impacts in several chemical disciplines, including chemical synthesis, drug discovery, catalysis, and materials science; see Table 1.

This review explores the recent advances in conformational analysis, emphasizing the integration of spectroscopic techniques, including NMR, IR, Raman, and UV-Vis, with QM computations such as DFT, *ab initio*, and coupled-cluster approaches. This work highlights the significant impact of the QM-spectral combination across several fields, including materials research, drug development, and catalysis. A review of recent developments in QM methods for conformational studies will be conducted. The article reviews recent case studies that illustrate how this combined approach has yielded significant insights into conformational analysis. Finally, this review will subsequently address the challenges associated with this topic, offering a framework for future research in this field.

Table 1 Impacts of the integrated QM-experimental approach in different fields.

Field	Combined approach	Examples of impacts	Ref.
Organic/ Inorganic synthesis	QM/NMR/ IR/UV-Vis	• Support the structure investigated of novel compounds. • Regioselectivity and thermodynamically preferred reaction route. • Assigning the preferred coordination sites of ligands in metal complexes and studying structural isomerism.	[26-28]
Drug discovery	QM/MD/X-ray/NMR/ TD-DFT/ ECD	• Identifying bioactive conformations of drug candidates • Refining H-atom positions in protein active sites (e.g., hydrogen-bond networks in enzymes). • Resolving the dynamics of drug molecules in lipid bilayers.	[1-3]
Natural products	QM/NMR/ TD-DFT /ECD	• Structural elucidation of natural products. • Determination of the absolute configuration. • Mechanisms involved in natural product biosynthesis.	[24, 29]
Catalysis	QM/MD/ IR/Raman/ IRC	• Evaluation of multiple reaction pathways and identification of transient intermediates. • Elucidating transition-state geometries using Intrinsic Reaction Coordinate (IRC) calculations.	[4, 5]
Materials Science	DFT/ TD-DFT/IR/ UV-Vis	• Characterization of novel polymers and nanomaterials. • Designing organic semiconductors with tailored optoelectronic properties.	[6-8]

2. Conformational Analysis and Its Significance

Conformational analysis is a central aspect of structural chemistry that explores the spatial arrangements of atoms within a molecule and the differences in their energies. Molecular conformations denote different three-dimensional arrangements of atoms in a molecule that maintain the same covalent connectivity and can be classified into rotational isomers and cyclic conformations. The rotational isomers arise from the rotation around single bonds, exemplified by the conformers analyzed for L-histidine methyl ester [30], as illustrated in Figure 1. Whereas, cyclic conformations are formed due to ring puckering in cyclic molecules such as the three conformers (Figure 2) investigated for 1,3-dimethyl-2-imidazolidinone due to the flexibility of the five-membered ring [31]. Molecular conformations exist in dynamic equilibrium, with populations determined by their relative Gibbs free energies (ΔG) and temperature (T) according to the Boltzmann distribution [32]. The conformational landscape can be represented as a potential energy surface (PES), covering all possible conformations along with their relative stabilities [17].

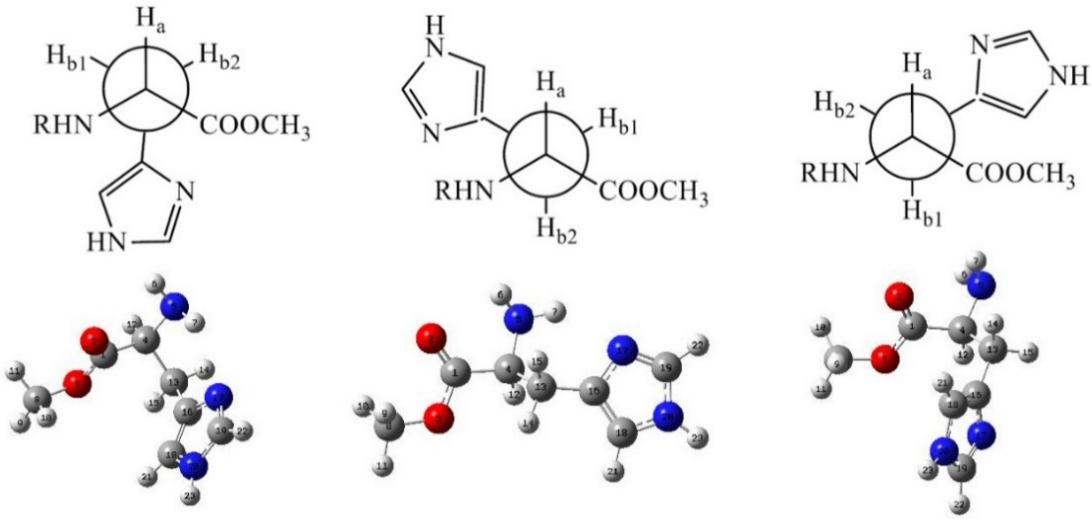


Figure 1 Newman projections representing the three rotational isomers (Top) of L-histidine methyl ester, R=H and their optimized geometries (bottom) at ωB97X-D/aug-cc-pVTZ level reported by Ref. **[30]**.

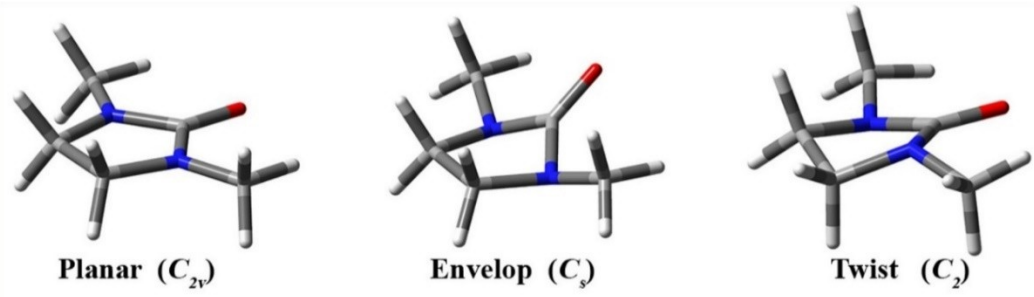


Figure 2 Equilibrium geometries of the proposed cyclic conformers of 1,3-Dimethyl-2-imidazolidinone using the MP2/6-311++G (d,p) calculations [31].

In 1932, Mizushima and Higasi began the historical development of conformational analysis by reporting the existence of *anti* and *gauche* conformers in 1,2-dichloroethane supported by Raman spectroscopy [33]. Barton significantly contributed in the 1950s by applying conformational analysis to cyclohexane derivatives, establishing a foundation for its use in natural product chemistry [34]. During the 1960s and 1970s, conformational analysis expanded into multiple disciplines, notably in the examination of cycloalkanes and alkaloids, emphasizing the distinct characteristics of each compound class [34, 35]. During the 1990s, techniques such as principal component analysis and essential dynamics analysis were developed to examine protein conformational ensembles, associating conformational alterations with functional mechanisms [36]. From the beginning of the year 2000, conformational analysis has experienced notable growth, primarily attributed to advancements in computational methods. The precision and efficiency of conformational studies improved significantly through the integration of experimental approaches and advanced computational methods. The

advancement of computational tools has enhanced researchers' understanding of molecular behavior and interactions, enabling them to analyze complex molecular systems [36, 37].

The stability of molecular conformers is influenced by several factors, including steric effects, intramolecular interactions, and environmental conditions. These factors collectively affect the energy landscape and the favored conformations in different environments. The stability of conformers is notably influenced by intramolecular hydrogen bonds; for example, N–H···O=C bonds increase the stability of *cis*-Amide conformers in proline-rich peptides [38]. Ring strain is a significant factor influencing the conformational preferences of cyclic molecules, such as cyclohexanes, which adopt chair conformations to reduce angle strain [39]. The stability of conformers is also affected by the orientation of substituents, such as axial and equatorial configurations. For example, 5-methyltetrahydro-1,3-oxazine favors an equatorial methyl group [40]. Concerning the environmental effect, the *gauche* conformer of butyronitrile exhibits greater stability under specific conditions of temperature and pressure [41].

Assessing conformational preferences is crucial for understanding molecular behavior, as slight structural alterations can substantially impact function. The study of molecular conformations is significant across various fields, such as drug discovery, molecular biology, materials science, and catalysis. Conformational analysis is essential in the design of drug molecules, as it identifies the optimal conformation for binding to a target protein [3]. The synthesis of natural products such as vitamin B12 highlights the significance of managing conformational preferences to attain specific chemical reactivities and biological activities [42], where conformational design principles are utilized to attain specific molecular structures. For enzymatic catalysis, studying conformational changes is vital for understanding enzyme mechanisms and developing inhibitors. These changes could overcome trade-offs between substrate specificity and product release, thereby enhancing catalytic efficiency [43]. In peptides, exploring the conformational preferences can inform the development of drugs that exhibit improved potency and selectivity. The incorporation of 2,3-methanopipecolic acids in peptides significantly increases the prevalence of the *cis* isomer, which can mimic proline's role in biological processes and assist in the design of novel bioactive compounds [44].

Conformational analysis has significance in material science, shown by its applications in many fields, including organic semiconductors, liquid-crystal, polymers, and metal-organic frameworks (MOFs). Using the 3D electron diffraction (3D ED), Ph-anti-benzothieno[5,6-b]benzothieno[3,2-b]thiophene, a novel organic semiconductor, exhibited complex conformational polymorphisms that influence its crystallization behavior and potential applications [45]. The exploration of liquid crystalline materials is facilitated by advanced computational techniques for rapid conformational analysis, enabling the development of new materials with specific properties [46]. Conformational

analysis elucidates the relationship between polymer structure and properties, facilitating the design of polymers with tailored characteristics for specific applications [47]. The porosity and surface area of MOFs are significantly influenced by the conformation of organic linkers, which are essential for applications such as catalysis and adsorption [48].

Conformational analysis provides valuable insights into molecular structures and dynamics; however, several critical unresolved issues remain. These include the accurate consideration of solvent effects [49], the handling of flexible structures with over ten rotatable bonds [50], and the prediction of temperature-dependent populations [51]. Recent advancements in machine learning force fields [52] and improved sampling techniques [53] are addressing these challenges, facilitating a more comprehensive exploration of conformational spaces.

3. Quantum Mechanical (QM) Methods

QM calculations are the cornerstone of computational chemistry, serving as a crucial tool for predicting and understanding the electronic structure and properties of molecules and materials [54], therefore aligning with both experimental and theoretical methodologies. Recent developments in computer hardware and software have greatly improved the potential of computational chemistry, allowing for more intricate and precise simulations [55]. Commonly used software packages for QM calculations include Gaussian [56], QChem [57], GAMESS [58], Psi4 [59], and NWChem [60]. All these software offer similar fundamental functionalities, with notable distinctions related to their user-friendliness, efficiency, and accessibility (free or commercial). The primary QM methods involve *ab initio* approaches (such as Hartree-Fock and post-Hartree-Fock), semiempirical methods, and DFT, each possessing its own characteristics and applications. The integration of QM with MM in QM/MM methods has broadened the applicability of QM calculations to larger and more complex systems.

Computational chemistry has progressed significantly since the first accurate simulations of gas-phase small molecules [61], shown by the receipt of two Nobel Prizes. In 1998, Walter Kohn and John Pople were awarded the first prize for their pioneering contributions to the development of DFT [62] and computational techniques in quantum chemistry [63]. The second prize was awarded in 2013 for the advancements of computational QM/MM models that simulate complex biological systems [64-66]. Currently, the extensive application of computational chemistry in medical and materials research is feasible [67, 68] due to advancements in methodologies and computational capabilities.

3.1 *Ab initio* Calculations

Ab initio calculations, derived from the Latin term meaning "from first principles" are QM methods that solve the Schrödinger equation without the use of empirical parameters, depending exclusively on fundamental physical constants. *Ab initio* Hartree-Fock (HF) calculations involve the approximation of the total molecular wavefunction Ψ as a Slater determinant of occupied spin orbitals.

The spatial orbitals are expressed as a linear combination of basis functions. HF calculations recover the bulk (≈99%) of the total electronic energy but neglects electron correlation[69], which is typically a few tenths of a hartree for small molecules (≈ 0.37 E_h for water). Because this missing energy is comparable to or larger than the energy differences of chemical interest, HF errors in reaction energies, barrier heights and non-covalent interactions can reach tens of kcal/mol, and harmonic frequencies are systematically overestimated by ~10% [70].

Post-HF approaches, including Møller-Plesset perturbation theory (MP), configuration interaction (CI), and coupled cluster (CC) methods, provide better treatment of electron correlation. These approaches methodically calculate electron correlation energy, necessary for precise electronic structure computations [71]. *Ab initio* calculations are employed to calculate molecular geometries, energies, vibrational frequencies, and spectra. These properties are crucial for understanding chemical reactions and interactions, including enzyme-substrate binding and reaction equilibrium [69].

3.2 Density Functional Theory (DFT)

DFT is currently one of the most widely used and well-established QM techniques for calculating electronic structures because it achieves an excellent compromise between computational cost and accuracy [72]. This theory is based on the Hohenberg-Kohn theorems, which state that all ground state properties of a system are determined by its electron density [62]. The practical applications of DFT involve approximations such as LDA and meta-GGA, especially concerning the exchange-correlation energy, a fundamental part of the theory. The precision of DFT calculations is significantly dependent on the selection of the exchange-correlation functional, and research continues to advance the development of more accurate functionals [73]. Recent advancements include hybrid and double-hybrid functionals, such as B3LYP [74, 75] and ωB97XD [76, 77], which enhance the accuracy of electronic structure predictions. Additionally, dispersion corrections, including DFT-D3 [76] and DFT-D4 [78] are applied for weak interactions in flexible molecules.

The HF theory has several deficiencies and inadequately describes most chemical reactions [70]. Both MP and CI methods provide accurate electronic energies for small atoms and molecules using large basis sets; however, they become too computationally expensive for larger systems. Modern DFT approaches offer greater precision compared to HF calculations with lower computational costs (Figure 3). Thus, DFT is preferred in handling large systems effectively, which makes it appropriate for investigating complex materials and biological systems. Owing to this effectiveness, DFT calculations have been extensively applied in cooperative experimental and computational studies [19].

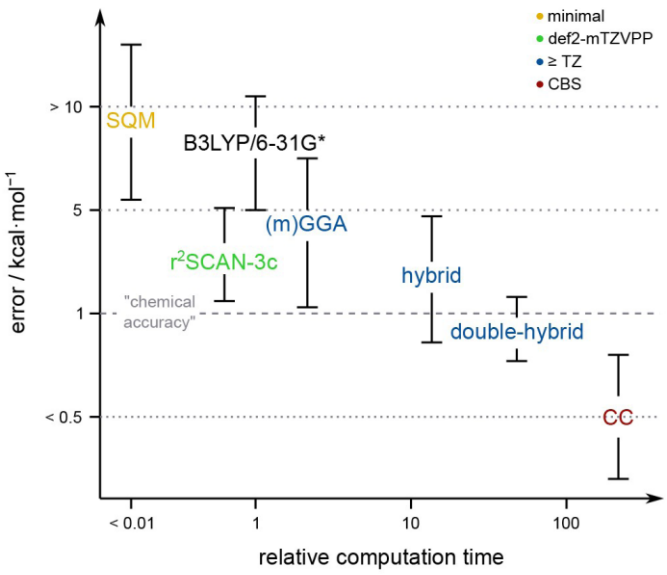


Figure 3. Accuracy in typical thermochemical applications vs. computation time (logarithmic scale) for common quantum chemistry methods [79].

3.3 General considerations in QM calculations

In computational chemistry, it is essential to deal with computational requirements with methodological accuracy and reliability. To achieve this objective, it is crucial to know the advantages/limitations of various approaches, consider the system size, and recognize the targeted properties, including structures, reaction energies, and conformational energies. Identifying suitable theoretical frameworks is essential for precisely characterizing a chemical system. Bursch and coworkers [79] have delineated important aspects to consider when conducting QM computations, the most notable of which are as follows:

1. A key issue in DFT is the selection of the exchange-correlation energy functional; hence, it is advisable to choose a functional carefully, considering the specific chemical system and the job at hand, rather than relying on popularity.
2. The application of the atomic-orbital basis set is essential. The key characteristic of basis sets is their completeness (size), which refers to the number of functions used to represent an electron. An appropriate basis set size (≥ triple-zeta; TZ) is crucial for energy-related features. It is essential to consider polarization functions for flexibility beside diffuse functions for anions, dipole moments, and polarizabilities. Finally, implement efficient core potentials for heavy elements (Z>36).
3. An additional significant aspect is the system's structural flexibility. Highly flexible structures may not be adequately represented by a single molecular property, such as energy or NMR spectra. It is recommended to evaluate the accessibility of relevant conformers for a specific system via conformational analysis.

4. Structure optimizations represent the beginning step of most QM studies, typically starting from either experimental data or an initial estimate using semiempirical or force-field methodologies. The most common user errors involve initial structures and input mistakes that lead to incorrect charge, spin, or protonation states, significantly altering the results. Consequently, the input must be carefully verified prior to initiating the computational procedure.
5. The calculation of vibrational frequencies is essential for determining zero-point vibration energies and for making thermostatistical corrections to enthalpy and free energy. It is essential for predicting IR/Raman spectra. For structure optimization and vibrational frequency calculations, it is necessary to employ the same theory level, or alternatively, a second set of optimized structures derived from this lower level must be utilized.
6. The calculated electronic energies serve as the principal indicator for the examination of conformers, reaction energies, barriers, and noncovalent interactions. These computations need larger basis sets for convergent results compared to structures or frequencies.

The expected performance of the most commonly used methods for conformational energies, NMR shifts, vibrational spectra and electronic spectra is compared in **Table 2**, together with their relative computational cost and recommended applications.

Table 2. Comparison of the main QM methods for conformational energies and spectroscopic properties

Method	Conformer energies	NMR shifts	Vibrational spectra	Electronic spectra	Cost	Recommended use
B3LYP-D3(BJ)	Good with dispersion correction; poor without it for folded/π-stacked structures	Reliable with GIAO; widely used	Very good after scaling	Valence states good; charge-transfer (CT) and Rydberg states underestimated	Low	Routine geometries, frequencies, NMR
M06-2X	Good for non-covalent interactions; grid-sensitive	Good	Good (own scale factors)	Better than B3LYP for CT owing to 54% HF exchange	Low–moderate	Energetics of flexible/dispersion-bound systems
ωB97X-D	Good; built-in dispersion	Good	Good after scaling	Good for CT/Rydberg (range separation)	Low–moderate	General-purpose, ECD/UV-Vis
MP2 (DLPNO-MP2)	Good but overbinds π-stacking/dispersion	Improves difficult cases; costly	Good for small systems	Not applicable	Moderate–high	Check on DFT energies, small/medium systems
CCSD(T) / DLPNO-CCSD(T)	Reference quality (“chemical accuracy”)	Benchmark only	Limited by cost	EOM-CCSD as benchmark	Very high	Single-point energies on DFT geometries
TD-DFT	–	–	–	Typically 0.2–0.3 eV for valence states; larger errors for CT, Rydberg, double excitations	Moderate	UV-Vis/ECD of medium-large molecules

3.4 Time-Dependent Density Functional Theory (TD-DFT)

TD-DFT computations expand traditional DFT to include time-dependent systems, facilitating the calculation of electronic excited states using linear response theory [80]. The approach provides excitation energies (often within 0.2-0.3 eV of experimental values), oscillator strengths, and charge-transfer characteristics [81]. TD-DFT is widely employed to predict the electronic circular dichroism (ECD) and UV-Vis spectra (electronic transitions) of organic and biological molecular systems [17]. Additionally, it is utilized to calculate the optical spectra of semiconductors and insulators, considering the impact of excitons, which are bound electron–hole pairs [82]. In the field of photonics, TD-DFT is helpful in examining the interaction between light and electrons, a crucial aspect for the development of devices that merge photonics with electronics [83].

The accuracy of TD-DFT depends strongly on the functional and on the nature of the excited state. The 0.2–0.3 eV error typically quoted applies to low-lying valence excitations of organic molecules. Global hybrids such as B3LYP underestimate charge-transfer and Rydberg excitation energies, an issue partly cured by range-separated hybrids (CAM-B3LYP, ωB97X-D). In the adiabatic linear-response approximation, states with significant double-excitation character are missing, and near-degenerate states may be mixed or wrongly ordered, which directly affects the sign pattern of ECD spectra. Solvent effects are described by linear-response PCM only approximately and neglect specific interactions, vibronic structure and band broadening are usually replaced by empirical line shapes, and ECD spectra are highly sensitive to conformer populations. Benchmarking against wavefunction methods (EOM-CCSD, DLPNO-STEOM-CCSD), testing several functionals, and Boltzmann-averaging over conformers are therefore recommended.

3.5 Potential Energy Surface (PES) Scans and Conformational Analysis

The combination of potential energy surface (PES) scan and conformational analysis with QM calculations provides significant understanding into molecular behavior. PES scans assess the variations in the energy of a molecule as a function of its geometric parameters, such as bond lengths, angles, or dihedral angles, to identify stable conformations and transition states [17]. A relaxed PES scan involves incrementally altering a particular structural parameter of the molecule followed by geometry optimization at each scanning point. The scan of PES can be carried out in either one or multiple dimensions, based on the complexity of the molecule. PES scans are essential for analyzing molecular flexibility, reaction pathways, and torsional barriers [56]. Developments in algorithms (e.g., CREST, meta-dynamics) and hybrid QM/MM methodologies persistently enhance efficiency and precision [84].

The conformational study of *meso*-2,3-dimercaptosuccinic acid was documented by Shaaban *et al.* [22], indicating that the *trans* conformer was preferred based on the PES scan during internal

rotation around the central C–C bond, using B3LYP/6-31++G(d,p) calculations; refer to **Figure 4A**. The authors performed three PES scans for the *trans* conformer by rotating the *carboxyl*, *thiol*, and *hydroxyl* groups to explore additional conformers. Accordingly, the global minimum (**Figure 4B**) has the carbonyl *staggered* relative to the CCS angle but *trans* to C–H, whereas the O–H is positioned *cis* to the carbonyl, and the S–H is *trans* to C–H and *staggered* to the CCC angle.

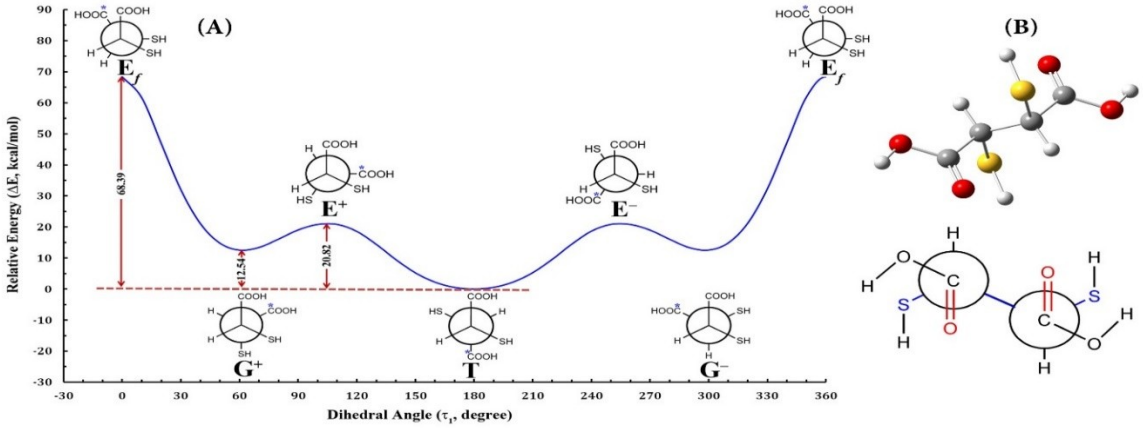


Figure 4. (A) PES scan during internal rotation around the central C–C bond for *meso*-DMSA obtained from B3LYP/6-311++G**[22]; **(B)** The global minimum for the *trans* conformer [22].

Employing B3LYP/6-311++G (d,p) calculations, Reference [31] documented a two-dimensional potential energy surface scan for 1,3-dimethyl-2-imidazolidinone by varying two dihedral angles (**Figure 5**) to determine the *planar*-to-*twist* barrier (42.6 kcal/mol).

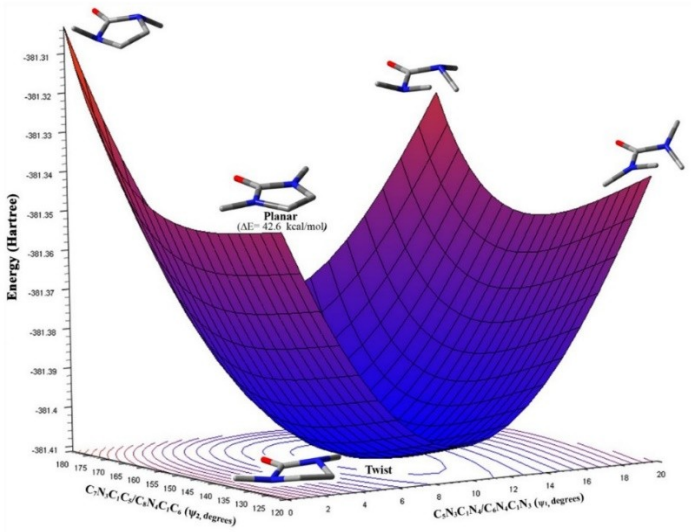


Figure 5. 2D-PES scan for ring puckering of 1,3-Dimethyl-2-imidazolidinone predicted from the B3LYP/6-311++G(d,p) calculations [31].

3.6 Machine Learning-Assisted Conformational Analysis

Machine learning (ML) is a crucial subset of artificial intelligence (AI) that focuses on the development of algorithms that allow computers to learn from data. This entails the application of statistical models for data analysis, pattern identification, and making predictions or decisions based on these patterns [85]. The use of ML in quantum mechanics calculations has revolutionized computational chemistry by accelerating the speed of accurate simulations and reducing computational costs. ML approaches, including neural networks, kernel methods, and Gaussian processes, are progressively used to predict molecular characteristics, optimize geometries, and substitute costly quantum mechanical calculations [86]. Grimme *et al.* developed a novel conformational searching approach, CREST, which offers a rapid alternative that rectifies inaccuracies seen in conventional conformational searching techniques [87]. CREST integrates the semiempirical GFN-xTB methods with metadynamics-based sampling to produce extensive conformational ensembles at a much-reduced cost compared to conventional *ab initio* techniques [88]. CREST is therefore not itself a machine-learning method, but an automated, semiempirical sampling tool that is often combined with ML-based refinement. The ML approaches relevant to conformational analysis are diverse and are best distinguished according to what the model predicts and how it is used. They can be classified into four categories: ML interatomic potentials/force fields, ML property prediction, ML–QM hybrids (Δ-learning), and ML-assisted conformational sampling, as summarised in **Table 3**. The main limitations of ML approaches should also be recognised: limited transferability beyond the training set, the scarcity of data for flexible and solvated systems, and the need for validation against QM calculations and experiment.

Table 3 Classification of machine-learning approaches used in conformational analysis

Category	Description	Examples
ML interatomic potentials / force fields	Neural-network or kernel potentials trained on DFT data to provide near-DFT energies and forces at force-field cost	ANI-2x [89], AIMNet2 [90], MACE-OFF [91]
ML property prediction	Models predicting spectra or shifts directly from structure or from low-level QM descriptors	iShiftML [110], CASCADE [92], DP4-AI [93]
ML–QM hybrids (Δ-learning)	ML corrects a cheap QM method towards a higher level (e.g., DFT → CCSD(T))	Δ-ML approaches reviewed in [86]
ML-assisted conformational sampling	Generative or active-learning models proposing conformers; ML potentials driving MD/metadynamics. Non-ML reference: CREST (GFN-xTB) [87, 88]	Torsional diffusion [94], GeoMol [95]

4. Integration of Spectral Techniques with QM Calculations

Spectral techniques, such as NMR, IR, Raman, UV-Vis, and CD spectroscopy, are indispensable for structural elucidation. Recent advancements in these approaches have markedly improved our ability to investigate molecular structure and conformations with extraordinary accuracy in exploring complex structures. **Table 4** highlights advanced spectroscopic methods and their applications in conformational analysis, enabling future advancements in structural biology and materials science.

The combined use of spectroscopic techniques and computational chemistry has become a cornerstone of conformational analysis. This synergy allows researchers to investigate the molecular structures and interpret spectral data with high accuracy. Barone *et al.* identified many aspects that make QM calculations an indispensable tool in the field of molecular spectroscopy [16]. The precise interpretation of spectral data requires comprehensive computational analysis. For instance, analyzing an experimental vibrational spectrum of a flexible molecule involves QM calculations, followed by spectral predictions and simulations to ascertain the relevant conformers. Experimental spectroscopy aims to elucidate the structure and bonding of molecules, with measurements focused on the frequencies of light absorbed by the molecular system. Computational spectroscopy serves as a connection between experimental data and fundamental physical properties by offering theoretical frameworks that relate observable measurements to molecular characteristics. QM calculations and experimental spectroscopy can serve as benchmarks for one another. Experimental spectroscopy exhibits high sensitivity to the electronic structure of a system, making it an effective method for verifying the reliability and accuracy of theoretical predictions and validating quantum chemistry calculations [16].

Table 4 Advanced Spectroscopic Techniques in Conformational Analysis

Spectral Technique	Applications
Raman optical activity (ROA) and VCD	Determination of absolute configurations and predominant conformations of several chiral compounds in solution [96].
2D-IR Spectroscopy	Monitoring ultrafast conformational dynamics, including protein folding and ligand binding [97].
Tip-enhanced Raman Spectroscopy (TERS)	Investigation of the conformational heterogeneity present in single molecules [98].
Ultrafast NMR spectroscopy	Monitoring conformational changes in real-time [99].
Multidimensional NMR	The analysis of the conformations of complex biological molecules, including proteins and RNA [100]

In-Cell NMR Spectroscopy	Conformational investigation of protein *in situ* within living cells [101]
Single-Molecule Fluorescence Spectroscopy	Investigation of protein folding and dynamics, yielding insights into conformational states and their dynamics [102].
Synchrotron Radiation CD (SRCD)	Investigation the secondary structure of proteins to understand its conformational behavior and stability at various conditions [103].

4.1 Vibrational Spectroscopy (IR/Raman)

Vibrational spectroscopy, involving infrared (IR) and Raman spectroscopy, is employed to analyze the vibrational modes of molecules, providing valuable insights into their structural and chemical properties. QM approaches are crucial for the accurate interpretation of the vibrational spectrum, which aids in conformational study. DFT approaches, particularly those using hybrid functionals like B3LYP [74, 75] and dispersion-corrected variants such as ωB97XD [76, 77], effectively predict IR and Raman spectra, while the use of anharmonic corrections (VPT2) improves accuracy [104].

The objective of the frequency calculations is to assign vibrational motions to the observed IR/Raman band. Normal coordinate analysis (NCA) is a method that effectively aids in the interpretation of the vibrational spectrum through mathematical representations of molecular vibrations using internal coordinates, which are well-known to spectroscopists. The process involves constructing a set of symmetry coordinates derived from combinations of internal coordinates, followed by the application of methods such as Wilson's FG matrix method for NCA [105]. The predicted potential energy distribution (PED) in the NCA indicates the percentage contribution of each symmetry coordinate to the calculated wavenumbers. In 2013, Jamróz [106] developed the computer code VEDA , vibrational energy distribution analysis, which performs NCA directly from the output file of the widely utilized Gaussian package in quantum chemistry. According to findings by Mohamed *et al.* [21], this algorithm cannot provide adequate accuracy to deliver comprehensive vibrational assignments for all fundamentals due to neglect of symmetry elements while mixing molecular vibrations. A comparison between the experimental vibrational spectra and theoretical predictions was essential for accurate assignment of the observed Raman and IR bands, as well as for a thorough understanding of the molecular geometrical structure. Consequently, the theoretical IR/Raman spectra can be simulated utilizing vibrational frequencies, Raman scattering activities, and infrared intensities derived from QM calculations. The theoretical framework for simulating IR and Raman spectra was partially outlined by Mohamed *et al.* [107]. Shaaban and coworkers simulated the IR and Raman spectra for the most stable conformer of the *keto* 4-Methyl-2-hydroxyquinoline using DFT (B3LYP,

ωB97XD, and mPW1PW91) calculations with a 6–311+G(2d,p) basis set [108]. Agreement in band positions after scaling and agreement in band intensities are different criteria. Harmonic frequencies depend mainly on the potential-energy curvature and are corrected by scale factors, whereas IR intensities depend on dipole-moment derivatives and Raman activities on polarizability derivatives, which are more sensitive to the functional and basis set (diffuse functions are particularly important for Raman). The double-harmonic approximation ignores anharmonic effects such as Fermi resonances, which redistribute intensity. Experimental conditions also matter: Raman intensities depend on the excitation wavelength and temperature (calculated activities must be converted to scattering intensities), and IR spectra recorded as solids or by ATR are affected by intermolecular interactions, packing and band-shape distortions, while matrix isolation shifts bands. The choice of line shape and width in simulated spectra further changes apparent intensities. Thus, the weaker simulated intensities below 1600 cm^{-1} in **Figure 6**, caused by the very high computed ν(C=O) intensity (860 km/mol), reflect both calculation limits and solid-state effects.

4.2 Nuclear Magnetic Resonance (NMR) Spectroscopy

Nuclear magnetic resonance (NMR) is a principal method used to elucidate the molecular structure of organic molecules. QM computations are essential for the assignment of NMR spectra and the investigation of molecular conformations, especially for flexible and complex molecules [23]. DFT using the Gauge-Including Atomic Orbital (GIAO) methodology is a widespread QM technique applied to calculate NMR parameters, such as chemical shifts and spin-spin coupling constants [104]. The DP4+ probability method is a significant technique that combines QM calculations with NMR data to improve the accuracy of conformational predictions [109]. In the context of structural elucidation, the implementation of ML models, such as the iShiftML, in computational NMR has resulted in exceptional accuracy in predicting chemical shifts at significantly reduced computational costs, thereby enhancing the correlation between experimental and calculated data to ascertain the most probable structures [110].

Comparative analyses of experimental and computationally predicted values for NMR chemical shifts and coupling constants have been utilized in various structural elucidation challenges. These include the determination of relative stereochemistry in flexible organic compounds [111], elucidation and reassignment of natural product structures [112], identification of byproducts in synthetic reactions [113], inference of macromolecular conformations in cyclic peptides [114], and correction of misassignments in the literature [115]. Shen *et al.* conducted a recent study analyzing literature from the past decade, identifying over 200 cases of misassigned natural compounds [116]. NMR misassignment errors constituted the most common type of mistake, representing 23% of the total errors [117].

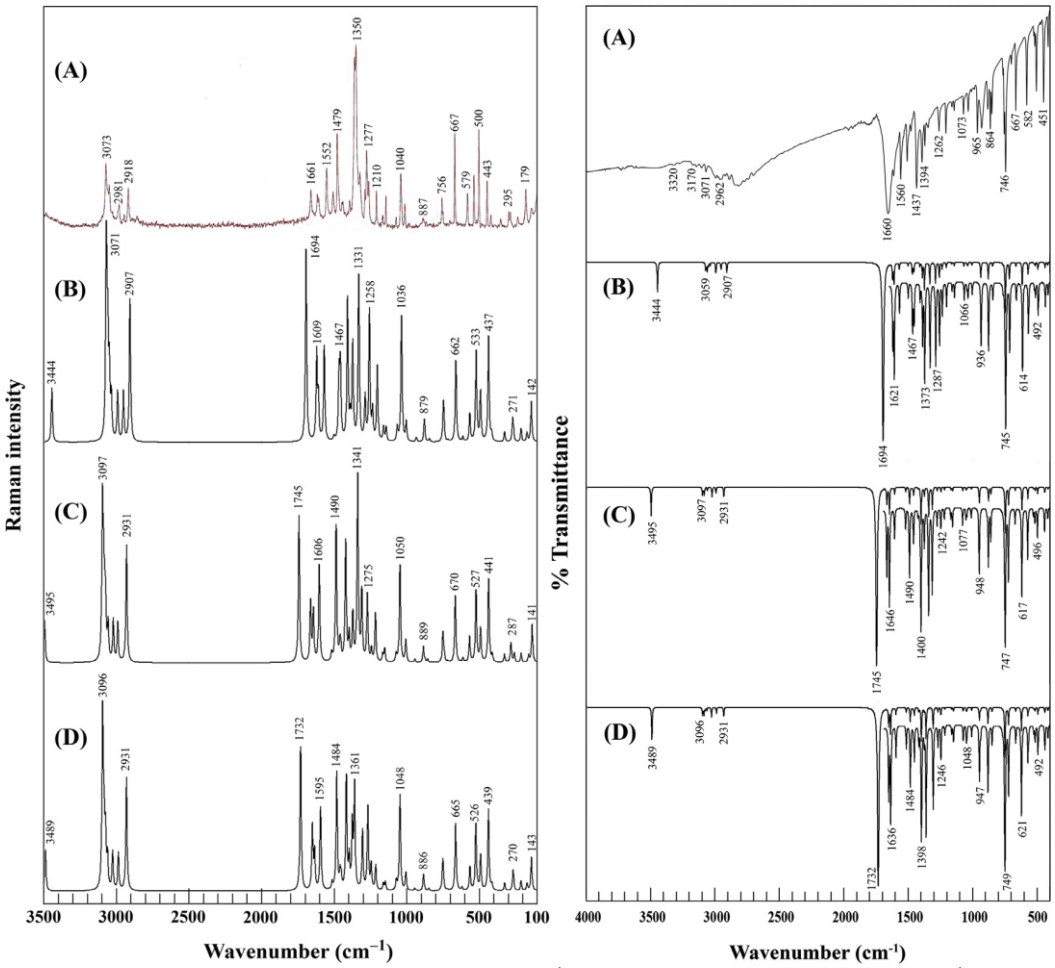


Figure 6. Experimental Raman (left, 3500–100 cm^{-1}) and IR (right, 4000−400 cm^{-1}) spectrum of 4-Methyl-2-hydroxyquinoline (A) compared to the simulated spectrum for *keto*- MQO using scaled frequencies from B3LYP (B), ωB97XD (C) and mPW1PW91 (D) methods at 6–311+*G* (2d,p) basis set [108].

Hexacyclinol is a natural product recognized as a significant example of utilizing NMR calculations for structural reassignment and elucidation. After its isolation and initial investigation of the molecular structure (**Figure 7A**), La Clair *et al.* in 2006 presented a total synthesis of hexacyclinol [118]. However, the measured NMR spectra of the synthetic product were inconsistent with the initially proposed structure, resulting in a controversy within the literature. Resolution was achieved when Rychnovsky proposed a revised structure (**Figure 7B**) according to calculations of ^{13}C NMR chemical shifts [119]. That year, this structure was validated using total synthesis and X-ray crystallography [120]. This case illustrates that the calculation of NMR parameters can effectively prevent the misassignment of natural product structures, thereby conserving valuable time and resources that would then be spent on total synthesis for structural elucidation [112, 121].

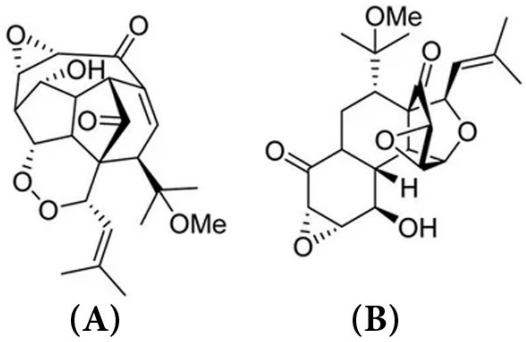


Figure 7. Originally proposed (A) and revised (B) structure of hexacyclinol [112].

4.3 UV-Vis and CD Spectroscopy

Ultraviolet-visible (UV-Vis) spectroscopy is a key analytical method employed to investigate electronic transitions in molecules, offering information about their electronic structure and conjugation. TD-DFT calculations with functionals such as B3LYP and CAM-B3LYP lead to accurate predictions of UV-visible spectra by calculating vertical electronic transitions and oscillator strengths, resulting in peak locations (λ_{max}) and intensities (ε), respectively [104]. Wavefunction-based approaches, like EOM-CCSD, provide enhanced precision for complex systems, but at a higher computational cost [122]. Electronic circular dichroism (ECD) spectroscopy is an effective chiroptical method for determining the absolute configuration of chiral molecules through the measurement of differential absorption of left- and right-circularly polarized light [123]. ECD spectra exhibit significant sensitivity to molecular conformation, thereby requiring TD-DFT calculations for different conformers to aid in precise assignments [124].

The UV-Vis spectral study of tetrahydroquinolines (THQs) revealed that TD-DFT effectively assigned long-wavelength absorption bands to $\pi \rightarrow \pi^*$ transitions, showing strong correlation with experimental findings [125]. The investigation of cyclohexane derivatives indicated that TD-DFT effectively simulates far-ultraviolet (FUV) spectra, elucidating the influence of *axial* and *equatorial* substitutions on electronic transitions, essential for comprehending conformational preferences [126]. The absolute configuration of racemic chlorpheniramine was found via chiral HPLC analysis and TD-DFT [127]. TD-DFT computations were used to examine the UV and CD spectra of selenium/tellurium chelates, yielding insights into their chiroptical characteristics [128].

5. Case Studies

This section presents four carefully selected cases in which spectral analysis, along with QM computations, yields precise conformational analysis.

The four case studies were selected because they (i) pair a quantitative experimental observable with calculations at an explicitly stated level of theory, (ii) together cover the main spectroscopic probes discussed in Section 4 (vibrational, including matrix-isolation, NMR chemical shifts and *J*-

couplings, and chiroptical ECD/OR), (iii) span different molecular classes (organosilicon ring, small conjugated nitrile, a flexible drug, and a natural product) and (iv) illustrate different outcomes, namely agreement with the lowest-energy conformer (Sections 5.1–5.2) and cases in which the global minimum was not the experimentally observed species (Sections 5.3–5.4). Section 5.2 is based on the authors' earlier work [21]; it was included because it provides a complete vibrational (NCA/PED) assignment.

5.1 1–chloro-1-chloromethylsilacyclohexane

Recent research by Stocka *et al.* (2022) on 1-chloro-1-chloromethylsilacyclohexane (1-Cl-1-ClMSiCH) illustrates the integration of vibrational spectroscopy (Raman, ATR-FTIR, and matrix isolation FTIR) and QM calculations for conformational analysis [129]. This study theoretically proposed 38 canonical conformers based on ring conformation (chair, boat, envelope, or skew-boat), the *axial*/*equatorial* positioning of the Si–Cl bond, and the *cis*/*trans*/*gauche* orientations of Cl and CH_2Cl. Using DFT-B3LYP and *ab initio*-MP2 calculations utilizing the aug-cc-pVTZ basis set, the authors determined that the chair axial *trans* conformation (**Figure 8a**) represents the global energy minimum structure. With an energy increase of 1.04 kcal/mol, the chair equatorial *trans* conformer was the second most stable, followed by axial *gauche* (1.39 kcal/mol) and equatorial *gauche* (1.65 kcal/mol). Owing to the small energy differences, the authors stated that all four lowest energy chair conformers (**Figure 8**) coexist at room temperature, confirmed by the experimentally observed vibrational spectra. Through the comparison of experimental spectra with the calculated spectra of various conformers, the researchers successfully assigned specific bands to the four lowest energy chair conformers [129].

Figure 9 presents the ATR-FTIR and Raman spectra, along with those calculated for the most stable conformers. From ATR FTIR spectrum, the existence of the equatorial *trans* and axial *gauche* conformers is evidenced by weak shoulder observed at 791 cm^{-1} and the shape of the right slope of the 777 cm^{-1} band. The observed Raman band at 753 cm^{-1} supports the presence of low energy conformers, as no calculated axial *trans* conformer bands are found at this wavenumber. The authors performed matrix isolation experiments to clarify the overlapping bands in the ATR-FTIR spectrum. The matrix isolation spectra are shown in **Figure 10**, particularly in the 900-500 cm^{-1} range, where significant discrepancies among the computed spectra of the four conformers are evident.

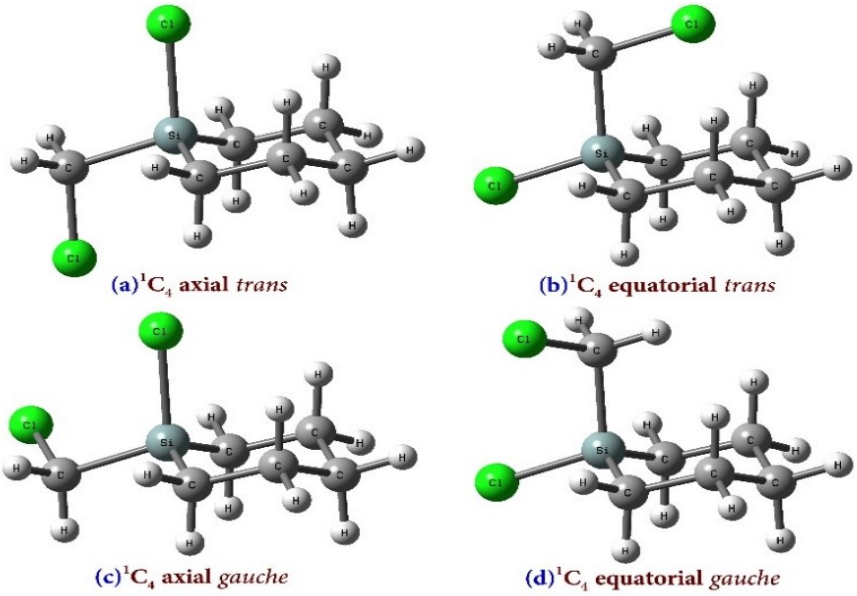


Figure 8. Chair conformers of the 1-Cl-1-ClMSiCH in axial/equatorial, *trans/gauche* conformation [129].

Three distinct bands were identified in the IR spectra of Ne/N_2 matrices at 804 cm^{-1}, 786 cm^{-1}, and 772 cm^{-1}, which are identified to the axial *trans* conformer and assigned to ring deformation modes and Si-C stretching. The very strong IR band detected at 778 cm^{-1} in nitrogen and 780 cm^{-1} in neon matches the calculated wavenumber of 786 cm^{-1} for the equatorial *gauche* conformer, attributed to the stretching vibrations of Si−C and C−C bonds.

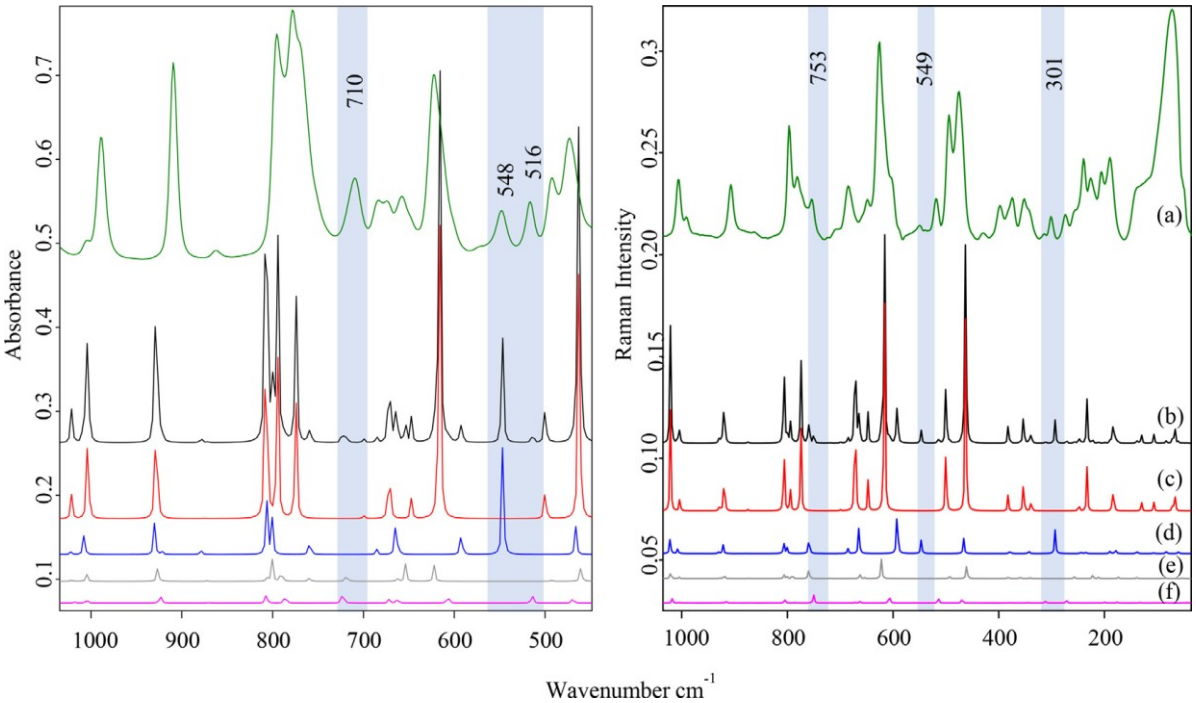


Figure 9. a) ATR (left) and Raman (right) experimental spectra of 1-Cl-1-ClMSiCH, calculated spectra of b) all conformers, c) axial *trans*, d) equatorial *trans*, e) axial *gauche*, f) equatorial *gauche*. This figure taken from Ref. [129].

The authors predicted the abundance of conformers by analyzing the integral intensity ratios of the spectral bands associated with different conformers. The nitrogen matrix concentrations are as follows: 81.3% for axial *trans*, 12.2% for equatorial *trans*, 2.6% for axial *gauche*, and 3.9% for equatorial *gauche*. The values are in qualitative agreement with those theoretically computed using the Boltzmann distribution at room temperature: 73%, 12%, 9%, and 6%, respectively. However, the theoretical populations (73/12/9/6%) differ appreciably from the matrix-derived ones, since matrix deposition may freeze non-equilibrium populations.

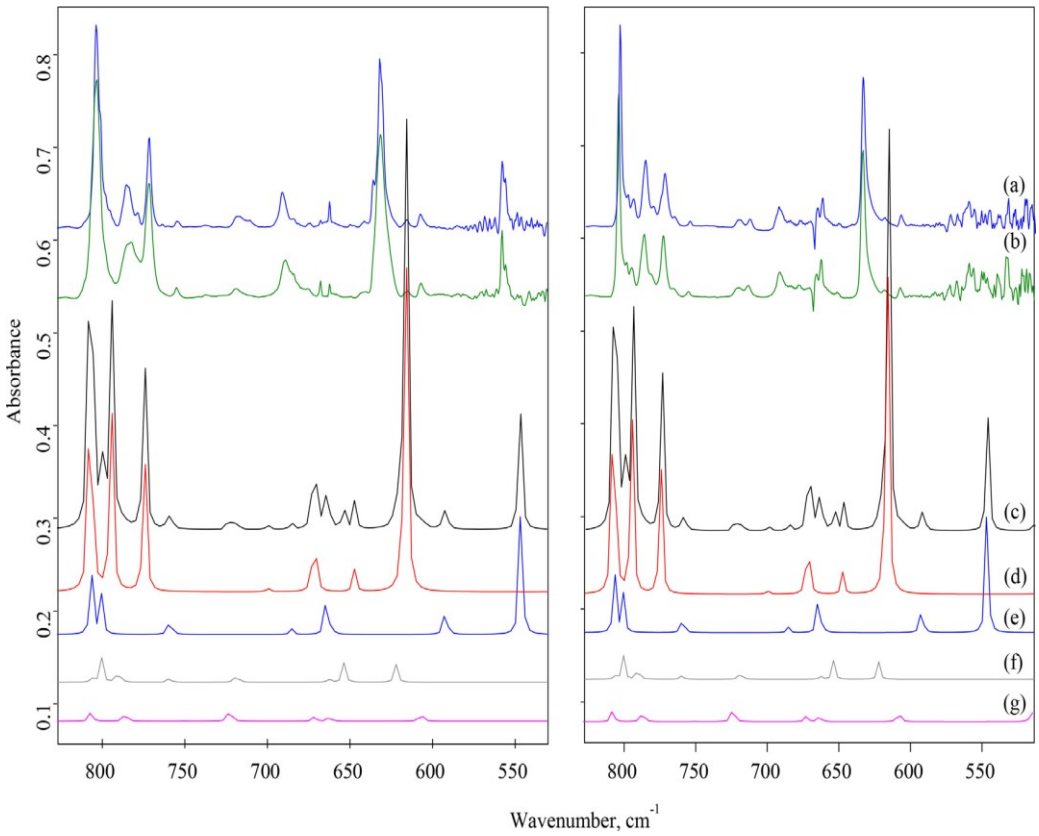


Figure 10 Infrared absorption spectra of 1-Cl-1-ClMSiCH isolated in neon at 3 K (left panel) and nitrogen (right panel) at 17 K, (b) after annealing at 9 K for neon and 35 K for nitrogen; and calculated spectra of (c) all conformers, (d) axial *trans*, (e) equatorial *trans*, (f) axial *gauche*, (g) equatorial *gauche*. This figure taken from Ref. [129]**.**

5.2 Centrosymmetric (2Z,4Z)-Hexa-2,4-dienedinitrile

The conformational analysis and detailed vibrational (IR/Raman) assignment for centrosymmetric (2Z,4Z)-Hexa-2,4-dienedinitrile (HDDN) was reported by Mohamed *et al.* [21], supported by DFT and *ab initio* calculations. As shown in **Figure 11**, the authors proposed three conformers for HDDN that correspond to the C_{2h} (*trans*), C_{2v}, and C_2 (*gauche*) point groups, attributed to the internal rotations around the central C−C single bond. DFT (B3LYP, M05-2X, and M06-2X) and *ab initio* (MP2 and MP4) calculations utilizing 6-31G(d) and 6-311+G(d,p) basis sets indicated

that the *trans* HDDN (C_{2h}) is the most stable conformer. The C_{2v} and *gauche* (C_2) conformers were determined to be energetically less favorable than the most stable C_{2h} by 12.18–13.70 and 6.51–8.18 kcal/mol, respectively. The C_{2v} conformer was identified as a transition state characterized by an imaginary wavenumber. These findings are confirmed by PES scans for internal rotation around the central C–C bond. The preference for the C_{2h} conformer coincides well with Raman and IR spectral analysis.

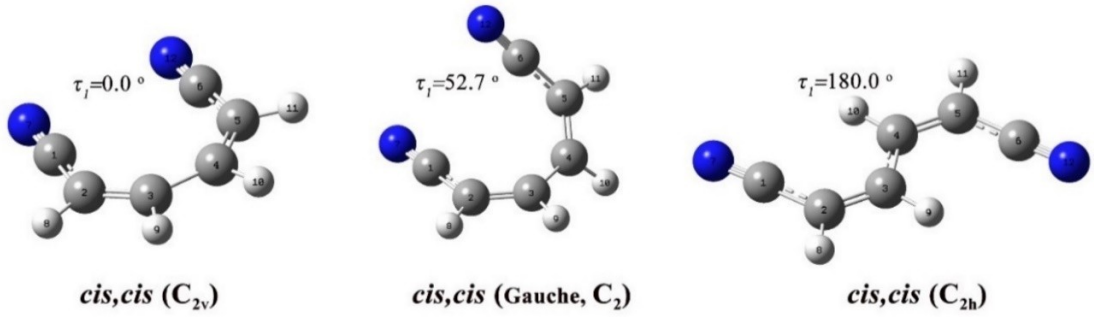


Figure 11. Equilibrium geometries of the proposed conformers of HDDN **[21]**.

This study confirmed the preference for the *trans* HDDN conformer in solution by comparing experimental and estimated spin-spin coupling constants [21]. The estimated/observed J value (H_9-H_{10}) of 10.19/10.8 Hz clearly supports the C_{2h} conformer in deuterated chloroform over the *gauche*-C_2 conformer (J = 4.81 Hz) after the exclusion of the transition state (C_{2v}).

The identification of the C_{2h} conformer was achieved through the analysis of observed Raman and IR spectra, in conjunction with the calculated vibrational frequencies. The single wavenumber is estimated at 999 cm^{-1} for the *trans* isomer, while three distinct estimated bands are observed at 998, 983, and 980 cm^{-1} for the *gauche* form. The strong Raman band observed at 962 cm^{-1} is neither split nor composite, indicating that it corresponds to the δ_{oop} C−H (ν_{12}) mode of the *trans* conformer. The authors presented comprehensive vibrational assignments of HDDN, utilizing NCA and PEDs in conjunction with calculated vibrational frequencies and force constants for the *trans* conformer exhibiting C_{2h} symmetry [21]. Consequently, 48 internal coordinates (**Figure 12**) were utilized to derive 42 symmetry coordinates (**Table 5**) employing the conventional Wilson GF method. Due to the mutual exclusion principle, we have categorized the thirty fundamental vibrations into 15 g modes (11 A_g + 4 B_g), which are only Raman active, and alone IR active 15 u modes (5 A_u + 10 B_u). **Tables 6/7** provide the observed Raman/IR bands along with their precise assignments to the normal modes of *trans* HDDN.

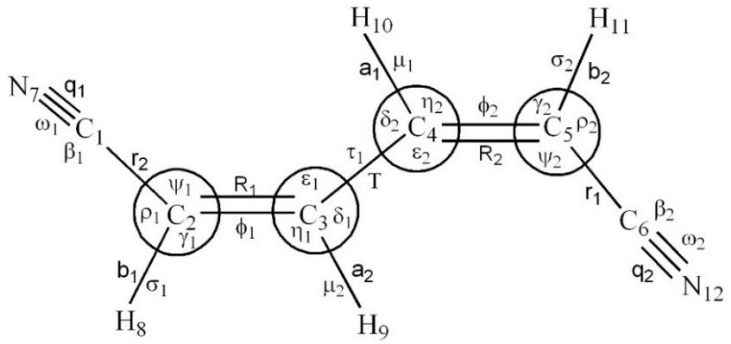


Figure 12. Atom numbering and internal coordinates definition of *trans* HDDN [21].

Table 5. Symmetry coordinates* for HDDN (*trans* conformer, C_{2h}) [21].

Species	ν_i	Definition	Symmetry coordinate*
A_g	ν_1	C–H symmetric stretch	$S_1 = a_1 + a_2 + b_1 + b_2$
	ν_2	C–H symmetric stretch	$S_2 = a_1 + a_2 - b_1 - b_2$
	ν_3	C≡N symmetric stretch	$S_3 = q_1 + q_2$
	ν_4	C=C symmetric stretch	$S_4 = R_1 + R_2$
	ν_5	C–$H_{terminal}$ *in-plane* bend	$S_5 = \rho_1 - \gamma_1 + \rho_2 - \gamma_2$
	ν_6	C–$H_{central}$ *in-plane* bend	$S_6 = \eta_1 - \delta_1 + \eta_2 - \delta_2$
	ν_7	C–$C_{central}$ stretch	$S_7 = T$
	ν_8	C–$C_{terminal}$ symmetric stretch	$S_8 = r_1 + r_2$
	ν_9	C=C–C *in-plane* bend	$S_9 = 2\varepsilon_1 - \eta_1 - \delta_1 + 2\varepsilon_2 - \eta_2 - \delta_2$
	ν_{10}	C–C≡N *in-plane* bend	$S_{10} = \beta_1 + \beta_2$
	ν_{11}	C=C–C *in-plane* bend	$S_{11} = 2\psi_1 - \rho_1 - \gamma_1 + 2\psi_2 - \rho_2 - \gamma_2$
B_g	ν_{12}	C–H *out-of-plane* bend	$S_{12} = \sigma_1 + \sigma_2 - \mu_1 - \mu_2$
	ν_{13}	C–H *out-of-plane* bend	$S_{13} = \sigma_1 + \sigma_2 + \mu_1 + \mu_2$
	ν_{14}	CCCC twist (C=C wag)	$S_{14} = \phi_1 - \phi_2$
	ν_{15}	C-C≡N *out-of-plane* bend (C–$C_{terminal}$ wag)	$S_{15} = \omega_1 - \omega_2$
A_u	ν_{16}	C–H *out-of-plane* bend	$S_{16} = \sigma_1 - \sigma_2 + \mu_1 - \mu_2$
	ν_{17}	C–H *out-of-plane* bend	$S_{17} = \sigma_1 - \sigma_2 - \mu_1 + \mu_2$
	ν_{18}	C-C≡N *out-of-plane* bend (C–$C_{terminal}$ wag)	$S_{18} = \omega_1 - \omega_2$
	ν_{19}	CCCC wag (C=C wag)	$S_{19} = \phi_1 + \phi_2$
	ν_{20}	C-$C_{central}$ torsion	$S_{20} = \tau_1$
B_u	ν_{21}	CH antisymmetric stretch	$S_{21} = a_1 - a_2 - b_1 + b_2$
	ν_{22}	CH antisymmetric stretch	$S_{22} = a_1 - a_2 + b_1 - b_2$
	ν_{23}	C≡N antisymmetric stretch	$S_{23} = q_1 - q_2$
	ν_{24}	C=C antisymmetric stretch	$S_{24} = R_1 - R_2$

Species	ν_i	Definition	Symmetry coordinate*
	ν_{25}	C–$H_{central}$ *in-plane* bend	$S_{25} = \eta_1 - \delta_1 - \eta_2 + \delta_2$
	ν_{26}	C–$H_{terminal}$ *in-plane* bend	$S_{26} = \rho_1 - \gamma_1 - \rho_2 + \gamma_2$
	ν_{27}	C-$C_{terminal}$ antisymmetric stretch	$S_{27} = r_1 - r_2$
	ν_{28}	C=C–$C_{terminal}$ antisymmetric bend	$S_{28} = 2\psi_1 - \rho_1 - \gamma_1 - 2\psi_2 + \rho_2 + \gamma_2$
	ν_{29}	C-C≡N antisymmetric bend	$S_{29} = \beta_1 - \beta_2$
	ν_{30}	C=C–$C_{central}$ antisymmetric bend	$S_{30} = 2\varepsilon_1 - \eta_1 - \delta_1 - 2\varepsilon_2 + \eta_2 + \delta_2$

*Symmetry coordinates are not normalized, for internal coordinates definitions, see **Figure 12**.

Table 6. Observed Raman bands and calculated symmetric wavenumbers (A_g and B_g) for *trans* HDDN [21].

Sp.	ν_i	Approximate description [a]	B3LYP/6-311+G(d,p)					Observed Raman
			Unscaled	Scaled [b]	R act. [c]	Rel. Int. [c]	PED	
A_g	ν_1	ν_s C–H	3187	3041	252	0.65	$87S_1$ $12S_2$	3050 sh, w
	ν_2	ν_s C–H	3166	3021	39.7	0.1	$88S_2$ 12 S_1	3045 w
	ν_3	ν_s C≡N	2321	2226	1171	5.14	$89S_3$ $11S_8$	2216 m
	ν_4	ν_s C=C	1665	1647	1405	10	$60S_4$ $20S_6$ $11S_7$	1613 vs
	ν_5	δ_{ip} C–H_{term}	1452	1395	21.8	0.19	$45S_5$ $32S_6$	-
	ν_6	δ_{ip} C–H_{cent}	1277	1230	336.6	3.41	$45S_6$ $23S_5$ $17S_7$ $28S_7$ $27S_5$ $11S_8$	1236 s
	ν_7	ν_s C–C_{cent}	1117	1093	8.5	0.1	$18S_9$	-
	ν_8	ν_s C–C_{term}	894	888	18.2	0.29	$60S_8$ $12S_4$ $12S_7$ $26S_9$ $22S_7$ $13S_{10}$	880 m
	ν_9	δ_{ip} C=C–C_{cent}	762	754	0.5	0.01	$28S_{11}$	-
	ν_{10}	δ_{ip} C-C≡N	407	404	6.7	0.3	$52S_{10}$ $32S_9$ $53S_{11}$ $13S_9$	403 m
	ν_{11}	δ_{ip} C=C–C_{term}	136	135	20.6	5.16	$32S_{10}$	156 m
B_g	ν_{12}	δ_{oop} C–H	999	999	13.2	0.18	$100S_{12}$	962 m
	ν_{13}	δ_{oop} C–H	819	819	2.8	0.05	$88S_{13}$	801 w
	ν_{14}	δ_{twist} CCCC	616	616	13.2	0.34	$84S_{14}$ $15S_{15}$	592 s
	ν_{15}	γ C–C_{term}	321	320	0.6	0.04	$63S_{15}$ $35S_{14}$	310 m

[a] Notations for fundamentals: s, symmetric; as, antisymmetric; ip, in-plane; ν, stretch; δ, bending and γ, wagging.
[b] Scaling factors of 0.91 and 0.90 for CH/C≡N stretches and δ_{ip} CH, respectively; 1.0 for heavy atom stretches and bends; 1.0 for γ CH.
[d] Calculated Raman activities in $Å^4$/mol. Relative intensities were scaled out of 10 from NCA.

Table 7. Observed infrared bands and calculated anti-symmetric wavenumbers (A_u and B_u) for *trans* HDDN [21].

Sp.	ν_i	Approximate description [a]	B3LYP					Observed IR
			Unscaled	Scaled [b]	IR int. [c]	Rel. Int. [c]	PED	
A_u	ν_{16}	δ_{oop} C–H	1025	1025	1	0.14	$100S_{16}$	982 m
	ν_{17}	δ_{oop} C–H	784	784	68.3	10	$71S_{17}$ $10S_{18}$ $60S_{18}13S_{17}$	750 vs
	ν_{18}	□ C–C_{term}	478	478	3.8	0.56	$32S_{19}$ $53S_{19}$ $25S_{18}$	468 s
	ν_{19}	τ CCCC	248	248	9.7	1.42	$18S_{20}$ $66S_{20}$	245 s
	ν_{20}	τ $CCCC_{cent}$	57	57	11.9	1.75	$10S_{17}23S_{19}$	-
B_u	ν_{21}	ν_{as} C–H	3189	3043	1.7	0.25	$97S_{21}$	3072 m
	ν_{22}	ν_{as} C–H	3174	3028	7.7	1.13	$98S_{22}$	3057 m
	ν_{23}	ν_{as} C≡N	2322	2227	39	5.71	$89S_{23}$ $11S_{27}$	2225/2213 s
	ν_{24}	ν_{as} C=C	1615	1606	4.7	0.69	$82S_{24}$	1573/1555 m
	ν_{25}	δ_{ip} C–H_{cent}	1381	1316	3.9	0.57	$54S_{25}$ $37S_{26}$	1346 m
	ν_{26}	δ_{ip} C–H_{term}	1233	1176	2	0.29	$53S_{26}$ $36S_{25}$	1200 s
	ν_{27}	ν_{as} C–C_{term}	965	955	11.8	1.73	$65S_{27}$	942 s
	ν_{28}	δ_{ip} C=C–C_{term}	644	638	1.1	0.15	$49S_{28}$ $26S_{29}$	632 s
	ν_{29}	δ_{ip} C-C≡N	328	325	0.3	0.04	$51S_{29}$ $42S_{30}$	323 s
	ν_{30}	δ_{ip} C=C–C_{cent}	100	99	16.4	2.4	$46S_{30}$ 35_{28} $20S_{29}$	-

[a] Notations for fundamentals: s, symmetric; as, antisymmetric; ip, in-plane; ν, stretch; δ, bending and γ, wagging.
[b] Scaling factors of 0.91 and 0.90 for CH/C≡N stretches and δ_{ip} CH, respectively; 1.0 for heavy atom stretches and bends; 1.0 for γ CH.
[c] Calculated infrared intensities in km/mol. Relative intensities were scaled out of 10 from NCA.

5.3 Chloroquine (CQ) drug

Hernandes and coworkers reported the conformational study of Chloroquine (CQ, **Figure 13**) in solution by DFT calculations and NMR spectral analysis in three solvents: water, chloroform, and DMSO [130]. CQ has served as a standard antimalarial drug since the early 1950s and has received approval from health authorities in certain countries for its experimental use in treating COVID-19. The authors investigated 30 trial conformers for CQ through a comprehensive conformational search, varying eight dihedral angles (as shown in **Figure 13**) to identify all plausible conformations that may exist in solution. A total of 30 proposed molecular conformations were fully optimized using the ωB97x-D/6-31G(d,p)-PCM calculations.

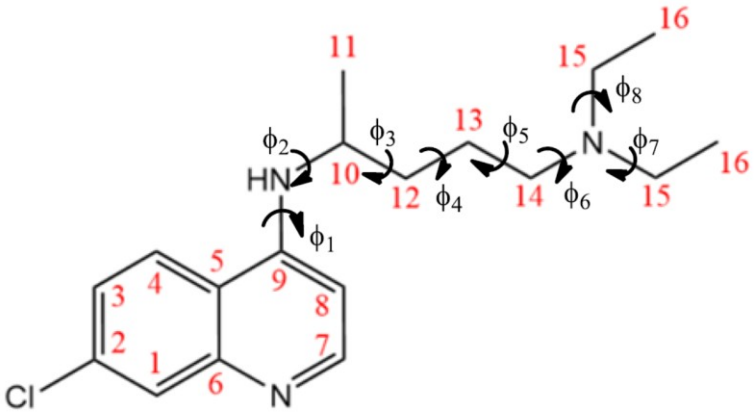


Figure 13. Structural formulas of chloroquine and the numbering adopted. Torsion angles (ϕ_1, ϕ_2, ϕ_3, ϕ_4, ϕ_5, ϕ_6, ϕ_7 and ϕ_8) are relevant for conformational analysis [130].

The optimized geometries for all suggested conformations (**M1-M30**) are shown in **Figure 14**. Using DFT calculations, ^{1}H NMR chemical shifts for **M1-M30** conformers were computed to identify the best match with those experimentally observed in solutions. The computational results indicate that conformer **M24** represents the global minimum-energy structure (lowest relative ΔG value) across all three solvents. It is stabilized by intramolecular hydrogen bonding between the hydrogen of the N−H group and a nitrogen atom attached to two alkyl groups.

The experimental ^{1}H NMR data were acquired in three deuterated solvents, D_2O, $CDCl_3$, and DMSO-d_6, which served as references for comparison with computed chemical shifts. This approach aims to identify the best correspondence with experimental results through the analysis of RMSD values and the experimental ^{1}H NMR profile. **Figure 15** illustrates the experimental ^{1}H NMR spectra in comparison with those computed for selecting optimized conformers. Accordingly, the global minimum-energy structure, **M24**, was not validated in all solvents owing to its inconsistent NMR profile, notably its undetected large chemical shift for N–H (~9 ppm). As shown in **Figure 15**, the optimized conformation **M12** demonstrates the most accurate alignment with the observed ^{1}H NMR profile in D_2O. However, structure **M8** exhibits a nearly perfect match with the experimental ^{1}H NMR spectrum in chloroform and DMSO (**Figure 16**), demonstrating the solvent's influence on conformational preferences. These findings indicate that, for chloroquine, spectroscopic analysis (NMR matching) was a more discriminating criterion than the calculated relative free energies for ascertaining solution-phase conformations, underscoring **M12** and **M8** as significant structures for forthcoming drug interaction investigations.

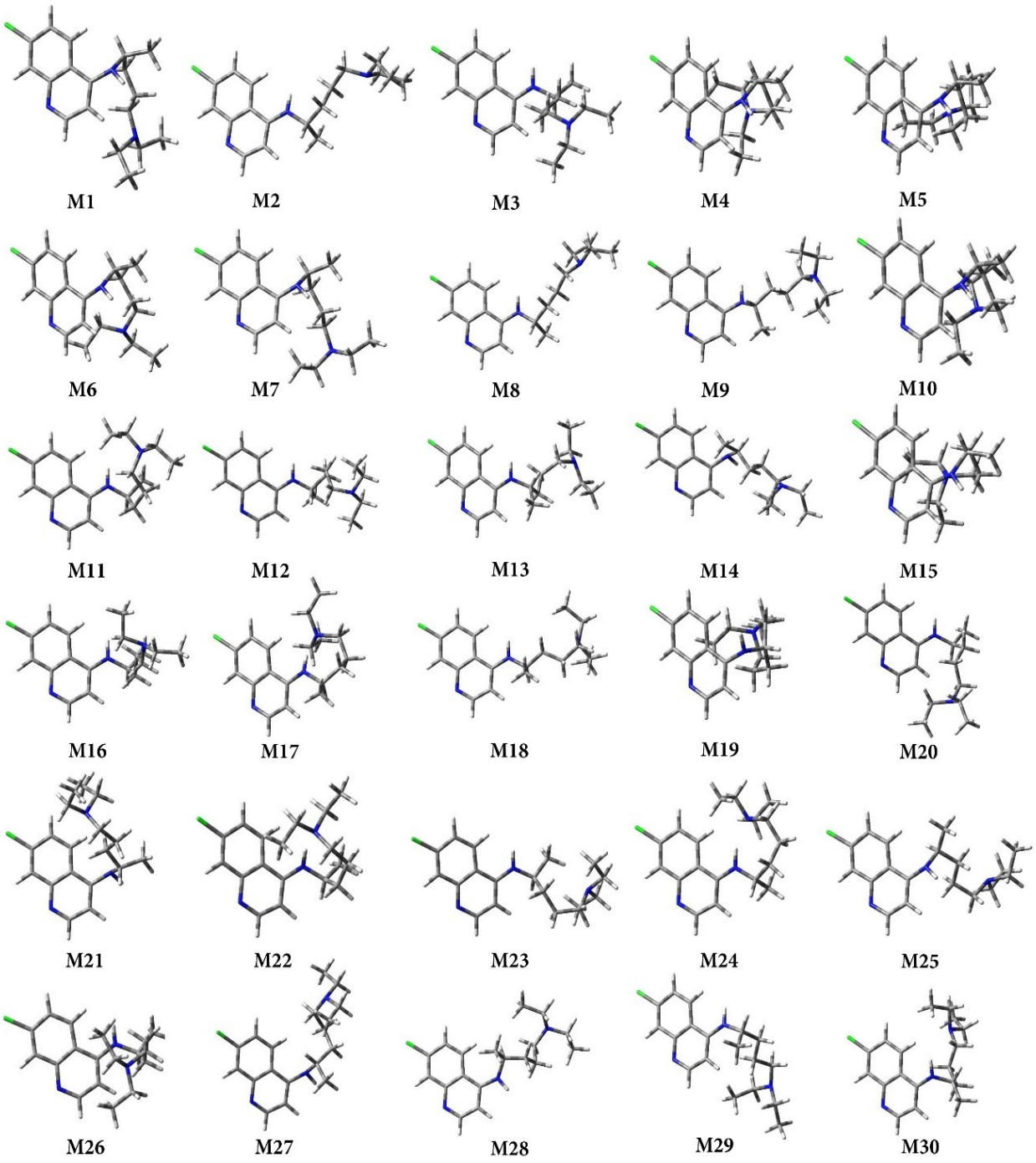


Figure 14. ωB97x-D/6-31G(d,p)-PCM-Water fully optimized structure of chloroquine (conformations **M1**–**M30).** This figure sketched using structure form supplement materials of Ref. [130]

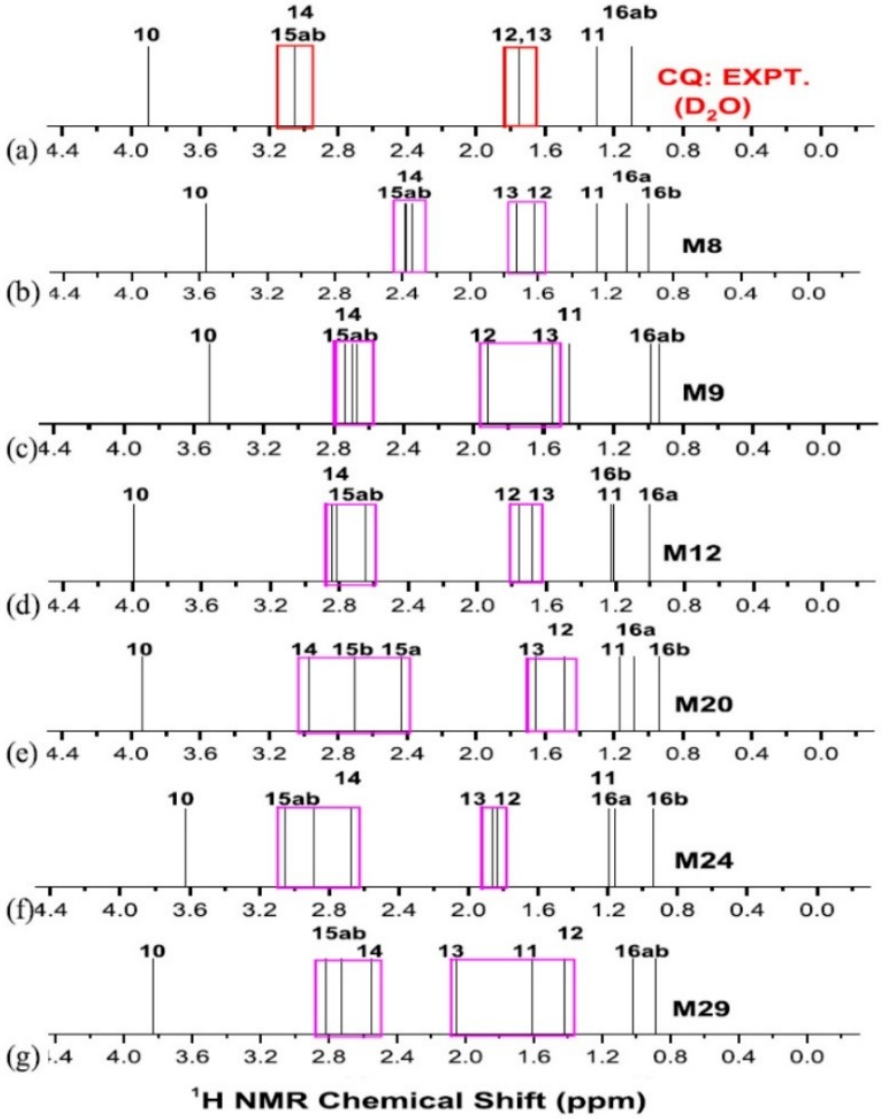


Figure 15. Experimental in D_2O (a) and B3LYP/6-31G(d,p)−PCM−water ^{1}H NMR spectra (b−g) for selected optimized structures of CQ. This figure taken from Ref. [130].

5.4 Absolute Configuration of Fusariumin A

The absolute configuration of Fusariumin A has been confirmed to be (2'R,3'R) through a combination of NMR techniques utilizing residual dipolar coupling (RDC) and chiroptical ECD spectroscopy, supported by TD-DFT calculations [131, 132]. Fusariumin A (**Figure 17A**) is an alkylpyrrole derivative extracted from the fungus Fusarium sp.

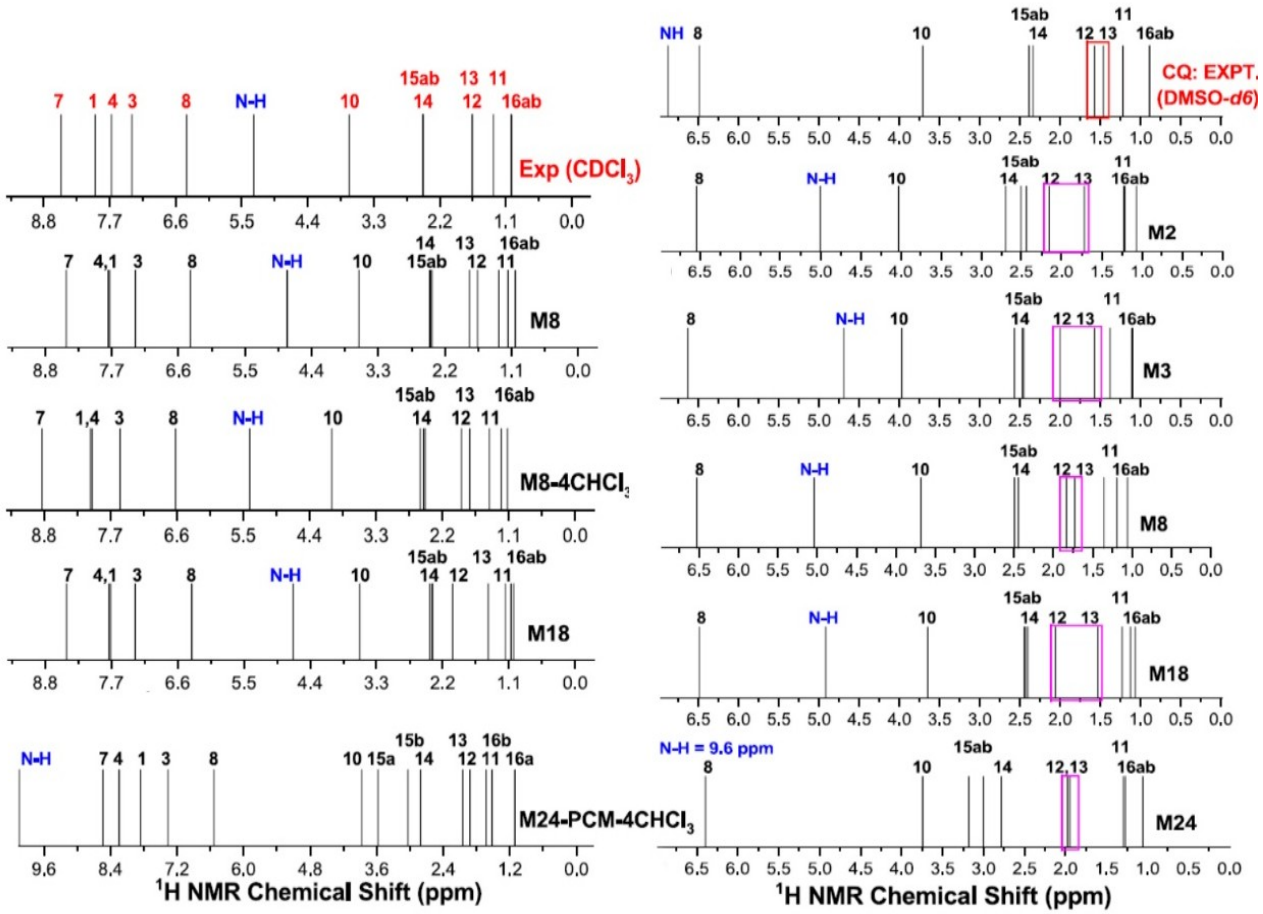


Figure 16. Experimental (left in $CDCl_3$; right in DMSO-d_6) and calculated ^{1}H NMR spectra for various optimized structures of CQ. This Figure taken from Ref. [130]

This compound includes two adjacent stereocenters within a flexible alkyl chain, and their relative configuration could not be established through conventional NMR methods. A systematic conformational search discovered the possible conformers of the 2'R,3'R diastereomer of Fusariumin A. Considering the high flexibility of the alkyl chains in Fusariumin A, this search focused solely on the rotations around the three bonds nearest to the stereocenters, while maintaining the two alkyl chains in the most stable all-*trans* conformation. The rotatable bonds included in the conformational search are indicated in red in Figure 17A. This technique yielded 12 conformers for the 2'R,3'R diastereomer. Of these, only conformer 11 (Figure 17C) demonstrated a satisfactory fit with the experimental RDCs and was consistent with all measured NOEs and J-couplings [131]. The conformer with the lowest energy, as determined by DFT calculations, was conformer **2**; nevertheless, it was incorrect since it did not correspond with the observed RDCs and NOEs (Figure 17B). Conformer **11** was the second-lowest energy structure, with an energy increase of 1.04 kcal/mol (ΔG = 1.1 kcal/mol). TD-DFT computations (B3LYP/6-31G*) were used to predict the ECD spectra of conformations **2** and **11** in DMSO employing the IEFPCM solvation model, in order to ascertain the exact configuration. The

predicted ECD spectrum for conformer **11** exhibited a negative ECD band that coincided closely with the experimental spectrum (**Figure 17D**), thus confirming the configuration of conformer **11** for natural Fusariumin A. The predicted ECD spectrum of conformer **2**, identified as the lowest energy conformer through DFT calculations, exhibits an opposite sign in comparison to that of conformer 11 (**Figure 17E**).

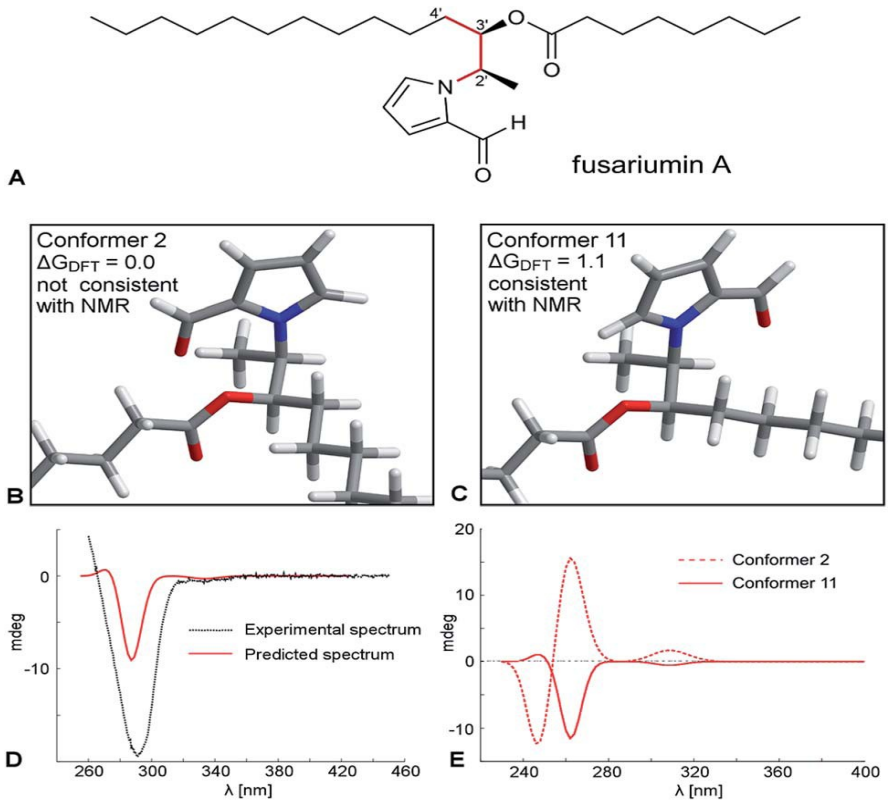


Figure 17. (A) Structure of Fusariumin A. (B) conformer **2** (C) conformer **11** (D) Experimental ECD spectrum of Fusariumin A as compared to the predicted ECD spectrum of the (2'R,3'R) enantiomer. (E) Predicted ECD spectra for Conformers **2** and **11**. This figure adapted from Ref. [132].

These findings have been verified by the optical rotation (OR) predictions at five distinct wavelengths. The anticipated OR values for conformer **11** closely aligned with the observed results, however those for conformer **2** had an opposite sign.

Populations follow from the Boltzmann distribution of relative free energies, so the energy type matters: electronic energies neglect vibrational and entropic contributions; Δ(E+ZPE) corrects for zero-point effects; and ΔG adds thermal enthalpy and entropy, normally from harmonic frequencies within the rigid-rotor/harmonic-oscillator approximation at the stated temperature. Low-frequency modes (<100 cm^{-1}) can introduce errors of several kcal/mol in entropy and are often treated with a quasi-harmonic correction. Because a 1 kcal/mol error changes a population ratio by a factor of ~5 at 298 K, for example, that the theoretical populations in Section 5.1 (73/12/9/6%) differ appreciably

from the matrix-derived ones (81.3/12.2/2.6/3.9%), since matrix deposition may freeze non-equilibrium populations.

These case studies, in particular chloroquine [130] and Fusariumin A [131, 132], show that agreement between Boltzmann-weighted calculated and experimental spectra is a necessary complement to, and in some cases a more discriminating criterion than, calculated relative energies. Calculated stabilities remain essential because they depend on the level of theory, the solvent model and the thermal corrections, whereas spectra may also mismatch for these same reasons. The most reliable assignments (e.g., DP4/DP4+ [32, 133], hexacyclinol [119, 120]) combine both criteria, and detailed protocols for the calculation of NMR chemical shifts are available [134].

6. Practical Guidelines for Method Selection

This section summarises typical starting points for selecting QM methods, basis sets and spectroscopic techniques for different classes of compounds **(Table 8).** These are typical starting points that should be validated against a higher-level reference for the system at hand.

Table 8. Practical guidelines for the selection of QM methods and basis sets

Task / property	Suggested level of theory	Suggested basis set	Key practical points
Conformer search	CREST (GFN2-xTB + metadynamics) or force-field/MD; then DFT re-optimisation	GFN2-xTB; then def2-SVP / 6-31G(d,p)	Use an energy window of ~5–6 kcal/mol; remove duplicates; check convergence for >10 rotatable bonds
Geometry + frequencies	Hybrid or range-separated hybrid DFT with dispersion (B3LYP-D3(BJ), ωB97X-D, M06-2X) or r^{2}SCAN-3c	Double-zeta with polarisation to def2-TZVP	Same level for optimisation and Hessian; confirm no imaginary frequencies; apply scale factors
Relative conformer energies	DLPNO-CCSD(T) or double-hybrid DFT single points on DFT geometries; dispersion-corrected hybrid DFT if cost-limited	Triple-/quadruple-zeta (def2-TZVPP, aug-cc-pVTZ) or CBS extrapolation	Include ZPE and thermal corrections to obtain ΔG; address BSSE (gCP/counterpoise)
NMR shifts and *J* couplings	GIAO with e.g. mPW1PW91, ωB97X-D or WP04 (^{1}H); DP4+ analysis	6-311+G(2d,p), def2-TZVP or pcS-*n*	Boltzmann-average all relevant conformers; implicit solvent matching the experiment; linear scaling
IR / Raman	Hybrid DFT (B3LYP-D3, ωB97X-D); VPT2 where anharmonicity matters	6-311+G(d,p), def2-TZVP (diffuse functions for Raman activities)	Compare frequencies and intensities separately; PED/NCA for assignment; matrix or solid-state effects
UV-Vis / ECD	TD-DFT with range-separated hybrids (CAM-B3LYP, ωB97X-D) or PBE0; EOM-CCSD / DLPNO-STEOM-CCSD for benchmarking	def2-TZVPD, aug-cc-pVDZ, 6-311+G(d,p)	Include enough states; Boltzmann-weight conformers; check charge-transfer character; implicit/explicit solvent

In terms of compound classes, small rigid organics are adequately treated by a single DFT workflow; flexible molecules and drug-like compounds require a conformer search plus Boltzmann averaging; chiral natural products need ECD/OR/NMR (DP4+) combined analysis; and metal complexes need functionals and effective core potentials benchmarked for the metal in question.

7. Challenges, Future Perspectives and Conclusions

Despite considerable advancements in the integration of conformational analysis, spectroscopic methods, and quantum mechanical (QM) computations, numerous challenges remain. Addressing these limitations is essential for improving accuracy, efficiency, and applicability in various chemical systems. A key challenge is the balance between accuracy and computational cost. Advanced QM methods involve CCSD and CASSCF, providing highly precise results; nonetheless, they are computationally expensive for large molecules with more than 50 atoms. DFT functionals, such as B3LYP, M06-2X, and ωB97XD, enable a reasonable balance; however, they may be inadequate for systems characterized by strong electron correlation or dispersion-dominated interactions [84]. Challenges continue also in the precise modeling of solvent effects and temperature-dependent behavior. Solvation models, such as PCM and SMD, provide approximations of bulk solvent effects while ignoring specific interactions between solute and solvent. Explicit solvent modeling, whether through molecular dynamics or QM/MM, enhances accuracy while also elevating computational requirements [135]. Most QM calculations assume static structures at absolute zero; however, spectroscopic properties are sensitive to temperature variations. Thermal fluctuations may be addressed by path-integral methods or MD [136]. QM approaches struggle with large-sized, flexible, or multi-component systems (e.g. biomolecules and supramolecular assemblies). Employing hybrid QM/MM and coarse-grained models helps the resolution of these challenges [137].

Implicit models (PCM, SMD, COSMO) are usually sufficient when the solvent is aprotic and weakly interacting (e.g., $CDCl_3$, CCl_4, cyclohexane), when the solute lacks strong hydrogen-bond donors/acceptors, and when relative energies of neutral conformers or non-exchangeable NMR shifts are the target. They become inadequate for (i) protic or strongly coordinating solvents (water, DMSO, alcohols) where specific hydrogen bonds or solvent bridges stabilise particular conformers, (ii) charged or zwitterionic species, (iii) exchangeable protons (N–H, O–H) whose chemical shifts depend strongly on hydrogen bonding, and (iv) chiroptical properties of chromophores with direct solute–solvent contacts. In these situations the cluster–continuum approach (a few explicit solvent molecules plus a continuum) is the minimum, with *ab initio*/classical MD sampling and averaging of QM properties over snapshots, or QM/MM, required when the solvation shell is dynamic. The chloroquine case (Section 5.3), where the N–H shift of the lowest-energy conformer **M24** was not observed experimentally, is a typical example in which specific solvent interactions may contribute to the mismatch.

Future research should integrate computational methods with experimental validation to improve conformational analysis and spectral predictions. QM methods and ML-accelerated calculations will enhance accuracy while minimizing computational costs. Hybrid QM/MM and

fragment-based methods will enable the study of large biomolecules and materials, while explicit solvation models and molecular dynamics will clarify the effects of solvent and temperature. Automated workflows that integrate machine learning, quantitative methods, and experimental data will enhance spectral interpretation, minimizing human bias and improving reproducibility. Innovations such as quantum computing and explainable AI present potential solutions for addressing complex chemical systems and dynamic processes. Collaborative efforts among computational chemists, spectroscopists, and data scientists are crucial for enhancing these methodologies, thereby maintaining their significance in drug discovery, materials science, and catalysis. Utilizing these advancements will allow researchers to achieve greater precision, faster predictions, and deeper understanding of molecular behavior.

Despite the progress summarised here, four issues limit the reliability of QM-assisted conformational analysis today. (i) Free-energy errors: conformer populations depend exponentially on ΔG (1 kcal/mol ≈ a factor of 5 at 298 K), yet errors of 1–2 kcal/mol remain common for flexible, dispersion-dominated systems and are amplified by harmonic, rigid-rotor thermal corrections. (ii) Solvent: implicit models cannot reproduce specific solute–solvent hydrogen bonding, as the chloroquine case shows; routine, affordable explicit-solvent or QM/MM-MD protocols are still lacking. (iii) Sampling: conformer searches for molecules with more than ~10 rotatable bonds are rarely converged, and results are seldom reported with convergence tests. (iv) Reproducibility: studies differ in functional, basis set, solvent model and thermal treatment, hampering comparison. We therefore recommend (a) benchmarking against a higher-level reference on a representative subset of conformers, (b) reporting Boltzmann-averaged rather than single-conformer spectra, (c) reporting the type of energy used for populations, and (d) depositing geometries and input files. Machine-learning potentials and automated workflows are the most promising route to meet these requirements, but they need rigorous, system-class-specific validation before they replace DFT in routine use.

The integration of spectroscopic techniques with QM computations has significantly revolutionized the field of conformational analysis, providing structural elucidation with an unprecedented degree of precision. Methods based on DFT calculations alongside NMR, IR, and UV-Vis spectroscopy offer reliable conformational insights for various compounds. Recent DFT functionals now provide precise predictions of NMR chemical shifts (within 0.1–0.2 ppm for ^{1}H NMR) and vibrational frequencies (within 5 cm^{-1} when anharmonic corrections are included). This review's case studies indicate that agreement between Boltzmann-weighted calculated and experimental spectra is a necessary complement to, and in some cases a more discriminating criterion than, calculated relative energies for ascertaining conformational preference among many feasible conformations; the

most reliable assignments combine both criteria. Prospective advancements in computational methodologies and machine learning are anticipated to further enhance these investigations, thereby increasing their applications in drug discovery, biochemistry, and materials science.

Funding

The authors declare that this research received no external funding.

Conflicts of Interest

The authors declare no conflict of interest.

References

[1] B. Dittrich, J. Lübben, S. Mebs, A. Wagner, P. Luger, and R. Flaig, "Accurate Bond Lengths to Hydrogen Atoms from Single-Crystal X-ray Diffraction by Including Estimated Hydrogen ADPs and Comparison to Neutron and QM/MM Benchmarks," Chemistry – A European Journal, vol. 23, no. 19, pp. 4605–4614, Mar. 2017, doi: 10.1002/chem.201604705.

[2] M. Monti, L. Biancorosso, and E. Coccia, "Time-Resolved Circular Dichroism in Molecules: Experimental and Theoretical Advances," Molecules, vol. 29, no. 17, p. 4049, Aug. 2024, doi: 10.3390/molecules29174049.

[3] G. J. Sharman, "Conformation and Stereochemical Analysis of Drug Molecules," eMagRes, pp. 105–116, Mar. 2015, doi: 10.1002/9780470034590.emrstm1392.

[4] S. G. Podkolzin, G. B. Fitzgerald, and B. E. Koel, "Combining Vibrational Spectroscopies with Quantum Chemical Calculations for Molecular-Level Understanding of Reaction Mechanisms on Catalytic Surfaces," Applications of Molecular Modeling to Challenges in Clean Energy, pp. 153–176, Jan. 2013, doi: 10.1021/bk-2013-1133.ch009.

[5] S. Maeda, Y. Harabuchi, Y. Ono, T. Taketsugu, and K. Morokuma, "Intrinsic reaction coordinate: Calculation, bifurcation, and automated search," International Journal of Quantum Chemistry, vol. 115, no. 5, pp. 258–269, Sep. 2014, doi: 10.1002/qua.24757.

[6] J. Anan, E. Adu Fosu, C. Obuah, M. Kojo Ainooson, A. Aniagyei, L. Hamenu, A. Oppong, A. Muller, "A DFT and TD-DFT studies of the photosensitizing capabilities of thiophene-based dyes," Computational and Theoretical Chemistry, vol. 1237, p. 114633, Jul. 2024, doi: 10.1016/j.comptc.2024.114633.

[7] H. Etabti, M. Er-Rajy, A. Fitri, A. Ammasi, M. Shkir, A.T. Benjelloun, M. Benzakour, M. McHarfi, "Computational Analysis of Triazolone-Based Dyes in DSSCs: Exploring Acceptor Terminal for Enhanced Photovoltaic Performance," Journal of Fluorescence, vol. 35, no. 10, pp. 9333–9357, Mar. 2025, doi: 10.1007/s10895-025-04231-z.

[8] R. Diana, U. Caruso, F. S. Gentile, L. Di Costanzo, P. Musto, and B. Panunzi, "Structural feature of thermo-induced fluorochromism in a 1D zinc coordination polymer. A cross-analysis by PL and FTIR spectroscopy, and DFT formalism," Dyes and Pigments, vol. 202, p. 110247, Jun. 2022, doi: 10.1016/j.dyepig.2022.110247.

[9] F. H. Allen, “The Cambridge Structural Database: a quarter of a million crystal structures and rising,” Acta Crystallographica Section B Structural Science, vol. 58, no. 3, pp. 380–388, May 2002, doi: 10.1107/s0108768102003890.

[10] James W. Robinson, Eileen Skelly Frame, George M. Frame II, “Introduction to Spectroscopy,” Undergraduate Instrumental Analysis, pp. 92–143, Jul. 2014, doi: 10.1201/b15921-6.

[11] J. Drenth, Principles of Protein X-Ray Crystallography. Springer New York, 2007. doi: 10.1007/0-387-33746-6.

[12] J. CAVANAGH, W. J. FAIRBROTHER, A. G. PALMER, M. RANCE, and N. J. SKELTON, “SEQUENTIAL ASSIGNMENT, STRUCTURE DETERMINATION, AND OTHER APPLICATIONS,” Protein NMR Spectroscopy, pp. 781–817, 2007, doi: 10.1016/b978-012164491-8/50012-9.

[13] B. Smith, “Spectral Interpretation Aids,” Infrared Spectral Interpretation, pp. 195–205, Feb. 2018, doi: 10.1201/9780203750841-9.

[14] A. D. Becke, “Density-functional thermochemistry. III. The role of exact exchange,” The Journal of Chemical Physics, vol. 98, no. 7, pp. 5648–5652, Apr. 1993, doi: 10.1063/1.464913.

[15] T. Bally and P. R. Rablen, “Quantum-Chemical Simulation of ¹H NMR Spectra. 2. Comparison of DFT-Based Procedures for Computing Proton–Proton Coupling Constants in Organic Molecules,” The Journal of Organic Chemistry, vol. 76, no. 12, pp. 4818–4830, May 2011, doi: 10.1021/jo200513q.

[16] V. Barone, S. Alessandrini, M. Biczysko, J.R. Cheeseman, D.C. Clary, A.B. McCoy, R.J. Dirisio, F. Neese, M. Melosso, C. Puzzarini, “Computational molecular spectroscopy,” Nature Reviews Methods Primers, vol. 1, no. 1, May 2021, doi: 10.1038/s43586-021-00034-1.

[17] J. H. Jensen, “Computational Chemistry,” Jan. 2017, doi: 10.14293/s2199-1006.1.sor-chem.clywqk5.v1.

[18] P. Atkins, J. de Paula, and J. Keeler, “Computational chemistry,” Atkins’ Physical Chemistry, Dec. 2022, doi: 10.1093/hesc/9780198847816.003.0049.

[19] G. Singh and S. Kumar, “Computational Chemistry: Exploring Molecular Properties and Reactivity,” Innovations in Science and Technology: Shaping a Sustainable Future (Vol. 1), pp. 87–97, May 2024, doi: 10.9734/bpi/mono/978-81-973809-6-9/ch8.

[20] J. Hénin, T. Lelièvre, M. R. Shirts, O. Valsson, and L. Delemotte, “Enhanced Sampling Methods for Molecular Dynamics Simulations [Article v1.0],” Living Journal of Computational Molecular Science, vol. 4, no. 1, p. 1583, Dec. 2022, doi: 10.33011/livecoms.4.1.1583.

[21] T. A. Mohamed, I. A. Shaaban, U. A. Soliman, and W. M. Zoghaib, “Computational studies, NMR, Raman and infrared spectral analysis of centrosymmetric (2Z,4Z)-Hexa-2,4-dienedinitrile,” Journal of Theoretical and Computational Chemistry, vol. 18, no. 02, p. 1950011, Mar. 2019, doi: 10.1142/s0219633619500111.

[22] I. A. Shaaban, A. Karoyo, L. D. Wilson, and T. A. Mohamed, “Raman and DRIFT spectra, vibrational assignments and quantum mechanical calculations of centrosymmetric meso -2,3-Dimercaptosuccinic acid,” Spectrochimica Acta Part A: Molecular and Biomolecular Spectroscopy, vol. 183, pp. 275–283, Aug. 2017, doi: 10.1016/j.saa.2017.04.017.

[23] G. Lauro, P. Das, R. Riccio, D. S. Reddy, and G. Bifulco, “DFT/NMR Approach for the Configuration Assignment of Groups of Stereoisomers by the Combination and Comparison of Experimental and Predicted Sets of Data,” The Journal of Organic Chemistry, vol. 85, no. 5, pp. 3297–3306, Jan. 2020, doi: 10.1021/acs.joc.9b03129.

[24] A. Mándi, J. Wu, and T. Kurtán, "TDDFT-ECD and DFT-NMR studies of thaigranatins A–E and granatumin L isolated from *Xylocarpus granatum*" RSC Advances, vol. 10, no. 53, pp. 32216–32224, 2020, doi: 10.1039/d0ra03725g.

[25] M. Habgood, T. James, and A. Heifetz, "Conformational Searching with Quantum Mechanics," Quantum Mechanics in Drug Discovery, pp. 207–229, 2020, doi: 10.1007/978-1-0716-0282-9_14.

[26] R. Fouad, I. A. Shaaban, T. E. Ali, M. A. Assiri, and S. S. Shenouda, "Co(ii), Ni(ii), Cu(ii) and Cd(ii)-thiocarbonohydrazone complexes: spectroscopic, DFT, thermal, and electrical conductivity studies" RSC Advances, vol. 11, no. 60, pp. 37726–37743, 2021, doi: 10.1039/d1ra06902k.

[27] I. A. Shaaban, T. E. Ali, M. A. Assiri, A. M. Fouda, S. M. Eledfawy, and N. M. Hassanin, "Regioselective cyclization reaction of 2-imino-2H-chromene-3-carboxamide with triethyl phosphonoacetate; a combined spectral and computational studies," Journal of Molecular Structure, vol. 1199, p. 126935, Jan. 2020, doi: 10.1016/j.molstruc.2019.126935.

[28] S. Bondock, T. Albarqi, I.A. Shaaban, M.M. Abdou, "Novel asymmetrical azines appending 1,3,4-thiadiazole sulfonamide: synthesis, molecular structure analyses, in silico ADME, and cytotoxic effect," RSC Advances, vol. 13, no. 15, pp. 10353–10366, 2023, doi: 10.1039/d3ra00123g.

[29] F.L.P. Costa, A.C.F. De Albuquerque, R.G. Fiorot, L.M. Lião, L.H. Martorano, G.V.S. Mota, A.L. Valverde, J.W.M. Carneiro, F.M. Dos Santos Junior, "Structural characterisation of natural products by means of quantum chemical calculations of NMR parameters: new insights," Organic Chemistry Frontiers, vol. 8, no. 9, pp. 2019–2058, 2021, doi: 10.1039/d1qo00034a.

[30] C. B. Braga and R. Rittner, "Combined Utilization of ^{1}H NMR, IR, and Theoretical Calculations To Elucidate the Conformational Preferences of Some l-Histidine Derivatives," The Journal of Physical Chemistry A, vol. 121, no. 3, pp. 729–740, Jan. 2017, doi: 10.1021/acs.jpca.6b12515.

[31] I. A. Shaaban, "Conformational analysis, infrared/Raman spectral assignment, and electronic structural studies of 1,3-dimethyl-2-imidazolidinone using quantum chemical calculations," Journal of Molecular Structure, vol. 1175, pp. 708–720, Jan. 2019, doi: 10.1016/j.molstruc.2018.08.015.

[32] S. G. Smith and J. M. Goodman, "Assigning Stereochemistry to Single Diastereoisomers by GIAO NMR Calculation: The DP4 Probability," Journal of the American Chemical Society, vol. 132, no. 37, pp. 12946–12959, Aug. 2010, doi: 10.1021/ja105035r.

[33] S. TOYOTA, "Discovery of internal rotation and conformers of 1,2-dichloroethane: the dawn of the concept of conformation," Proceedings of the Japan Academy, Series B, vol. 100, no. 2, pp. 101–113, Feb. 2024, doi: 10.2183/pjab.100.003.

[34] G. A. Morrison, "Conformational Analysis of Some Alkaloids," Fortschritte der Chemie Organischer Naturstoffe / Progress in the Chemistry of Organic Natural Products / Progrès dans la Chimie des Substances Organiques Naturelles, pp. 269–317, 1967, doi: 10.1007/978-3-7091-8164-5_9.

[35] V. Dragojlovic, "Conformational analysis of cycloalkanes," ChemTexts, vol. 1, no. 3, Aug. 2015, doi: 10.1007/s40828-015-0014-0.

[36] S. Hayward, "A Retrospective on the Development of Methods for the Analysis of Protein Conformational Ensembles," The Protein Journal, vol. 42, no. 3, pp. 181–191, Apr. 2023, doi: 10.1007/s10930-023-10113-9.

[37] Y. Zhou, I. Limbu, M. J. Garson, and E. H. Krenske, "Conformational Sampling in Computational Studies of Natural Products: Why Is It Important?," Journal of Natural Products, vol. 87, no. 10, pp. 2543–2549, Sep. 2024, doi: 10.1021/acs.jnatprod.4c00852.

[38] J. Jumper, R. Evans, A. Pritzel, T. Green, M. Figurnov, O. Ronneberger, K. Tunyasuvunakool, R. Bates, A. Žídek, A. Potapenko, A. Bridgland, C. Meyer, S.A.A. Kohl, A.J. Ballard, A. Cowie, B. Romera-Paredes, S. Nikolov, R. Jain, J. Adler, T. Back, S. Petersen, D. Reiman, E. Clancy, M. Zielinski, M. Steinegger, M. Pacholska, T. Berghammer, S. Bodenstein, D. Silver, O. Vinyals, A.W. Senior, K. Kavukcuoglu, P. Kohli, D. Hassabis, "Highly accurate protein structure prediction with AlphaFold," Nature, vol. 596, no. 7873, pp. 583–589, Jul. 2021, doi: 10.1038/s41586-021-03819-2.

[39] L. C. Allen, "Electronegativity is the average one-electron energy of the valence-shell electrons in ground-state free atoms," Journal of the American Chemical Society, vol. 111, no. 25, pp. 9003–9014, Dec. 1989, doi: 10.1021/ja00207a003.

[40] V. V. Kuznetsov, "Relative stability of 5-methyl- and 3,5-dimethyltetrahydro-1,3-oxazine conformers," Russian Journal of Organic Chemistry, vol. 52, no. 3, pp. 409–413, Mar. 2016, doi: 10.1134/s1070428016030192.

[41] M. I. Alomari, "Computational study of n-butyronitrile in gas and condensed phases: conformational relative stability and thermal properties," Journal of Chemical Sciences, vol. 130, no. 12, Nov. 2018, doi: 10.1007/s12039-018-1573-6.

[42] R. Chen, Y. Shen, S. Yang, and Y. Zhang, "Conformational Design Principles in Total Synthesis," Angewandte Chemie International Edition, vol. 59, no. 34, pp. 14198–14210, Jun. 2020, doi: 10.1002/anie.202003735.

[43] O. Rivoire, "A role for conformational changes in enzyme catalysis," Biophysical Journal, vol. 123, no. 12, pp. 1563–1578, Jun. 2024, doi: 10.1016/j.bpj.2024.04.030.

[44] L. Ricci, L. Sernissi, D. Scarpi, F. Bianchini, A. Contini, and E. G. Occhiato, "Synthesis and conformational analysis of peptides embodying 2,3-methanopipecolic acids," Organic & Biomolecular Chemistry, vol. 15, no. 32, pp. 6826–6836, 2017, doi: 10.1039/c7ob01617d.

[45] H. Kurokawa, S. Maki-Yonekura, K. Takaba, T. Higashino, S. Inoue, T. Hasegawa, K. Yonekura, "3D Electron Diffraction Structure of an Organic Semiconductor Reveals Conformational Polymorphism," Journal of the American Chemical Society, vol. 147, no. 7, pp. 5669–5678, Feb. 2025, doi: 10.1021/jacs.4c12734.

[46] J. Hobbs, C. J. Gibb, E. Cruickshank, R. Walker, and R. J. Mandle, "Rapid conformational analysis of semi-flexible liquid crystals," Liquid Crystals, vol. 51, no. 6, pp. 1022–1034, Apr. 2024, doi: 10.1080/02678292.2024.2333323.

[47] Y. Sasanuma, "Applications: Conformational Analysis and Elucidation of Structure–Property Relationships of Polymers," Conformational Analysis of Polymers, pp. 207–213, Mar. 2023, doi: 10.1002/9781119716655.part5.

[48] E. Sharmin and F. Zafar, "Introductory Chapter: Metal Organic Frameworks (MOFs)," Metal-Organic Frameworks, Oct. 2016, doi: 10.5772/64797.

[49] J. Tomasi, B. Mennucci, and R. Cammi, "Quantum Mechanical Continuum Solvation Models," Chemical Reviews, vol. 105, no. 8, pp. 2999–3094, Jul. 2005, doi: 10.1021/cr9904009.

[50] K. S. Watts, P. Dalal, R. B. Murphy, W. Sherman, R. A. Friesner, and J. C. Shelley, "ConfGen: A Conformational Search Method for Efficient Generation of Bioactive Conformers," Journal

of Chemical Information and Modeling, vol. 50, no. 4, pp. 534–546, Apr. 2010, doi: 10.1021/ci100015j.

[51] A. Fernandez-Ramos, B. A. Ellingson, B. C. Garrett, and D. G. Truhlar, "Variational Transition State Theory with Multidimensional Tunneling," Reviews in Computational Chemistry, pp. 125–232, Jan. 2007, doi: 10.1002/9780470116449.ch3.

[52] W. Plazinski, A. Plazinska, and A. Brzyska, "Efficient sampling of high-energy states by machine learning force fields," Physical Chemistry Chemical Physics, vol. 22, no. 25, pp. 14364–14374, 2020, doi: 10.1039/d0cp01399d.

[53] G. A. Tribello, M. Bonomi, D. Branduardi, C. Camilloni, and G. Bussi, "PLUMED 2: New feathers for an old bird," Computer Physics Communications, vol. 185, no. 2, pp. 604–613, Feb. 2014, doi: 10.1016/j.cpc.2013.09.018.

[54] I.N. Levine, "Quantum Chemistry. 7th Edition", Pearson Education, New York. 2014.

[55] D. G. Truhlar and V. Mckoy, "Computational chemistry," Computing in Science & Engineering, vol. 2, no. 6, pp. 19–21, Nov. 2000, doi: 10.1109/mcise.2000.881703.

[56] M.J. Frisch, G.W. Trucks, H.B. Schlegel, G.E. Scuseria, M.A. Robb, J.R. Cheeseman, G. Scalmani, V. Barone, G.A. Petersson, H. Nakatsuji, X. Li, M. Caricato, A.V. Marenich, J. Bloino, B.G. Janesko, R. Gomperts, B. Mennucci, H.P. Hratchian, J.V. Ortiz, A.F. Izmaylov, J.L. Sonnenberg, Williams, F. Ding, F. Lipparini, F. Egidi, J. Goings, B. Peng, A. Petrone, T. Henderson, D. Ranasinghe, V.G. Zakrzewski, J. Gao, N. Rega, G. Zheng, W. Liang, M. Hada, M. Ehara, K. Toyota, R. Fukuda, J. Hasegawa, M. Ishida, T. Nakajima, Y. Honda, O. Kitao, H. Nakai, T. Vreven, K. Throssell, J.A. Montgomery Jr., J.E. Peralta, F. Ogliaro, M.J. Bearpark, J.J. Heyd, E.N. Brothers, K.N. Kudin, V.N. Staroverov, T.A. Keith, R. Kobayashi, J. Normand, K. Raghavachari, A.P. Rendell, J.C. Burant, S.S. Iyengar, J. Tomasi, M. Cossi, J.M. Millam, M. Klene, C. Adamo, R. Cammi, J.W. Ochterski, R.L. Martin, K. Morokuma, O. Farkas, J.B. Foresman, D.J. Fox, in, Wallingford, CT, 2016.

[57] Y. Shao, Z. Gan, E. Epifanovsky, A.T.B. Gilbert, M. Wormit, J. Kussmann, A.W. Lange, A. Behn, J. Deng, X. Feng, D. Ghosh, M. Goldey, P.R. Horn, L.D. Jacobson, I. Kaliman, R.Z. Khaliullin, T. Kuś, A. Landau, J. Liu, E.I. Proynov, Y.M. Rhee, R.M. Richard, M.A. Rohrdanz, R.P. Steele, E.J. Sundstrom, H.L. Woodcock, P.M. Zimmerman, D. Zuev, B. Albrecht, E. Alguire, B. Austin, G.J.O. Beran, Y.A. Bernard, E. Berquist, K. Brandhorst, K.B. Bravaya, S.T. Brown, D. Casanova, C.-M. Chang, Y. Chen, S.H. Chien, K.D. Closser, D.L. Crittenden, M. Diedenhofen, R.A. Distasio, H. Do, A.D. Dutoi, R.G. Edgar, S. Fatehi, L. Fusti-Molnar, A. Ghysels, A. Golubeva-Zadorozhnaya, J. Gomes, M.W.D. Hanson-Heine, P.H.P. Harbach, A.W. Hauser, E.G. Hohenstein, Z.C. Holden, T.-C. Jagau, H. Ji, B. Kaduk, K. Khistyaev, J. Kim, J. Kim, R.A. King, P. Klunzinger, D. Kosenkov, T. Kowalczyk, C.M. Krauter, K.U. Lao, A.D. Laurent, K.V. Lawler, S.V. Levchenko, C.Y. Lin, F. Liu, E. Livshits, R.C. Lochan, A. Luenser, P. Manohar, S.F. Manzer, S.-P. Mao, N. Mardirossian, A.V. Marenich, S.A. Maurer, N.J. Mayhall, E. Neuscamman, C.M. Oana, R. Olivares-Amaya, D.P. O'Neill, J.A. Parkhill, T.M. Perrine, R. Peverati, A. Prociuk, D.R. Rehn, E. Rosta, N.J. Russ, S.M. Sharada, S. Sharma, D.W. Small, A. Sodt, T. Stein, D. Stück, Y.-C. Su, A.J.W. Thom, T. Tsuchimochi, V. Vanovschi, L. Vogt, O. Vydrov, T. Wang, M.A. Watson, J. Wenzel, A. White, C.F. Williams, J. Yang, S. Yeganeh, S.R. Yost, Z.-Q. You, I.Y. Zhang, X. Zhang, Y. Zhao, B.R. Brooks, G.K.L. Chan, D.M. Chipman, C.J. Cramer, W.A. Goddard, M.S. Gordon, W.J. Hehre, A. Klamt, H.F. Schaefer, M.W. Schmidt, C.D. Sherrill, D.G. Truhlar, A. Warshel, X. Xu, A. Aspuru-Guzik, R. Baer, A.T.

Bell, N.A. Besley, J.-D. Chai, A. Dreuw, B.D. Dunietz, T.R. Furlani, S.R. Gwaltney, C.-P. Hsu, Y. Jung, J. Kong, D.S. Lambrecht, W. Liang, C. Ochsenfeld, V.A. Rassolov, L.V. Slipchenko, J.E. Subotnik, T. Van Voorhis, J.M. Herbert, A.I. Krylov, P.M.W. Gill, M. Head-Gordon, "Advances in molecular quantum chemistry contained in the Q-Chem 4 program package," Molecular Physics, vol. 113, no. 2, pp. 184–215, Sep. 2014, doi: 10.1080/00268976.2014.952696.

[58] G.M.J. Barca, C. Bertoni, L. Carrington, D. Datta, N. De Silva, J.E. Deustua, D.G. Fedorov, J.R. Gour, A.O. Gunina, E. Guidez, T. Harville, S. Irle, J. Ivanic, K. Kowalski, S.S. Leang, H. Li, W. Li, J.J. Lutz, I. Magoulas, J. Mato, V. Mironov, H. Nakata, B.Q. Pham, P. Piecuch, D. Poole, S.R. Pruitt, A.P. Rendell, L.B. Roskop, K. Ruedenberg, T. Sattasathuchana, M.W. Schmidt, J. Shen, L. Slipchenko, M. Sosonkina, V. Sundriyal, A. Tiwari, J.L. Galvez Vallejo, B. Westheimer, M. Włoch, P. Xu, F. Zahariev, M.S. Gordon, "Recent developments in the general atomic and molecular electronic structure system," The Journal of Chemical Physics, vol. 152, no. 15, Apr. 2020, doi: 10.1063/5.0005188.

[59] R.M. Parrish, L.A. Burns, D.G.A. Smith, A.C. Simmonett, A.E. Deprince, E.G. Hohenstein, U. Bozkaya, A.Y. Sokolov, R. Di Remigio, R.M. Richard, J.F. Gonthier, A.M. James, H.R. McAlexander, A. Kumar, M. Saitow, X. Wang, B.P. Pritchard, P. Verma, H.F. Schaefer, K. Patkowski, R.A. King, E.F. Valeev, F.A. Evangelista, J.M. Turney, T.D. Crawford, C.D. Sherrill, "Psi4 1.1: An Open-Source Electronic Structure Program Emphasizing Automation, Advanced Libraries, and Interoperability," Journal of Chemical Theory and Computation, vol. 13, no. 7, pp. 3185–3197, Jun. 2017, doi: 10.1021/acs.jctc.7b00174.

[60] M. Valiev, E.J. Bylaska, N. Govind, K. Kowalski, T.P. Straatsma, H.J.J. Van Dam, D. Wang, J. Nieplocha, E. Apra, T.L. Windus, W.A. De Jong, "NWChem: A comprehensive and scalable open-source solution for large scale molecular simulations," Computer Physics Communications, vol. 181, no. 9, pp. 1477–1489, Sep. 2010, doi: 10.1016/j.cpc.2010.04.018.

[61] H. F. Schaefer, "Methylene: A Paradigm for Computational Quantum Chemistry," Science, vol. 231, no. 4742, pp. 1100–1107, Mar. 1986, doi: 10.1126/science.231.4742.1100.

[62] W. Kohn, "Nobel Lecture: Electronic structure of matter—wave functions and density functionals," Reviews of Modern Physics, vol. 71, no. 5, pp. 1253–1266, Oct. 1999, doi: 10.1103/revmodphys.71.1253.

[63] J. A. Pople, "Nobel Lecture: Quantum chemical models," Reviews of Modern Physics, vol. 71, no. 5, pp. 1267–1274, Oct. 1999, doi: 10.1103/revmodphys.71.1267.

[64] M. Karplus, "Citing 'Development of Multiscale Models for Complex Chemical Systems: From H+H2 to Biomolecules (Nobel Lecture)'," Angewandte Chemie International Edition, vol. 53, no. 38, pp. 9992–10005, Jul. 2014, doi: 10.1002/anie.201403924.

[65] M. Levitt, "Birth and Future of Multiscale Modeling for Macromolecular Systems (Nobel Lecture)," Angewandte Chemie International Edition, vol. 53, no. 38, pp. 10006–10018, Aug. 2014, doi: 10.1002/anie.201403691.

[66] A. Warshel, "Multiscale Modeling of Biological Functions: From Enzymes to Molecular Machines (Nobel Lecture)," Angewandte Chemie International Edition, vol. 53, no. 38, pp. 10020–10031, Jul. 2014, doi: 10.1002/anie.201403689..

[67] X. Dai and Y. Chen, "Computational Biomaterials: Computational Simulations for Biomedicine," Advanced Materials, vol. 35, no. 7, Dec. 2022, doi: 10.1002/adma.202204798.

[68] S. G. Louie, Y.-H. Chan, F. H. da Jornada, Z. Li, and D. Y. Qiu, "Discovering and understanding materials through computation," Nature Materials, vol. 20, no. 6, pp. 728–735, May 2021, doi: 10.1038/s41563-021-01015-1.

[69] E. G. Lewars, "Ab initio Calculations," Computational Chemistry, pp. 175–390, Sep. 2010, doi: 10.1007/978-90-481-3862-3_5.

[70] C.J. Cramer, "Essentials of Computational Chemistry: Theories and Models," Wiley, 2005.

[71] J. Townsend, J. K. Kirkland, and K. D. Vogiatzis, "Post-Hartree-Fock methods: configuration interaction, many-body perturbation theory, coupled-cluster theory," Mathematical Physics in Theoretical Chemistry, pp. 63–117, 2019, doi: 10.1016/b978-0-12-813651-5.00003-6.

[72] E. F. Silva-Júnior, T. M. Aquino, and J. X. Araújo-Júnior, "Quantum Mechanical (QM) Calculations Applied to ADMET Drug Prediction: A Review," Current Drug Metabolism, vol. 18, no. 6, Jul. 2017, doi: 10.2174/1389200218666170316094514.

[73] M. Aamir Iqbal, N. Ashraf, W. Shahid, D. Afzal, F. Idrees, and R. Ahmad, "Fundamentals of Density Functional Theory: Recent Developments, Challenges and Future Horizons," Density Functional Theory - Recent Advances, New Perspectives and Applications, May 2022, doi: 10.5772/intechopen.99019.

[74] A. D. Becke, "Density-functional exchange-energy approximation with correct asymptotic behavior," Physical Review A, vol. 38, no. 6, pp. 3098–3100, Sep. 1988, doi: 10.1103/physreva.38.3098.

[75] C. Lee, W. Yang, and R. G. Parr, "Development of the Colle-Salvetti correlation-energy formula into a functional of the electron density," Physical Review B, vol. 37, no. 2, pp. 785–789, Jan. 1988, doi: 10.1103/physrevb.37.785.

[76] J.-D. Chai and M. Head-Gordon, "Systematic optimization of long-range corrected hybrid density functionals," The Journal of Chemical Physics, vol. 128, no. 8, Feb. 2008, doi: 10.1063/1.2834918.

[77] J.-D. Chai and M. Head-Gordon, "Long-range corrected hybrid density functionals with damped atom–atom dispersion corrections," Physical Chemistry Chemical Physics, vol. 10, no. 44, p. 6615, 2008, doi: 10.1039/b810189b.

[78] E. Caldeweyher, J.-M. Mewes, S. Ehlert, and S. Grimme, "Extension and evaluation of the D4 London-dispersion model for periodic systems," Physical Chemistry Chemical Physics, vol. 22, no. 16, pp. 8499–8512, 2020, doi: 10.1039/d0cp00502a.

[79] M. Bursch, J.-M. Mewes, A. Hansen, and S. Grimme, "Best Practice DFT Protocols for Basic Molecular Computational Chemistry," Apr. 2022, doi: 10.26434/chemrxiv-2022-n304h.

[80] M. E. CASIDA, "Time-Dependent Density Functional Response Theory for Molecules," Recent Advances in Density Functional Methods, pp. 155–192, Nov. 1995, doi: 10.1142/9789812830586_0005.

[81] A. Dreuw and M. Head-Gordon, "Single-Reference ab Initio Methods for the Calculation of Excited States of Large Molecules," Chemical Reviews, vol. 105, no. 11, pp. 4009–4037, Oct. 2005, doi: 10.1021/cr0505627.

[82] J. R. Williams, N. Tancogne-Dejean, and C. A. Ullrich, "Time-Resolved Exciton Wave Functions from Time-Dependent Density-Functional Theory," Journal of Chemical Theory and Computation, vol. 17, no. 3, pp. 1795–1805, Feb. 2021, doi: 10.1021/acs.jctc.0c01334.

[83] B. Ait Hammou, A. El Kaaouachi, E. Hassan Mounir, H. Mabchour, A. El Oujdi, A. Echchelh, S. Dlimi, D. Ennajih, "DFT and TDDFT Calculations of Ground and Excited States of

Photoelectron Emission," Density Functional Theory - New Perspectives and Applications, Jan. 2024, doi: 10.5772/intechopen.111611.

[84] S. Grimme, "Exploration of Chemical Compound, Conformer, and Reaction Space with Meta-Dynamics Simulations Based on Tight-Binding Quantum Chemical Calculations," Journal of Chemical Theory and Computation, vol. 15, no. 5, pp. 2847–2862, Apr. 2019, doi: 10.1021 /acs.jctc.9b00143.

[85] M. Paluszek and S. Thomas, "An Overview of Machine Learning," MATLAB Machine Learning Recipes, pp. 1–19, 2024, doi: 10.1007/978-1-4842-9846-6_1.

[86] O. A. von Lilienfeld, K.-R. Müller, and A. Tkatchenko, "Exploring chemical compound space with quantum-based machine learning," Nature Reviews Chemistry, vol. 4, no. 7, pp. 347–358, Jun. 2020, doi: 10.1038/s41570-020-0189-9.

[87] S. Grimme, C. Bannwarth, S. Dohm, A. Hansen, J. Pisarek, P. Pracht, J. Seibert, F. Neese, "Fully Automated Quantum-Chemistry-Based Computation of Spin–Spin-Coupled Nuclear Magnetic Resonance Spectra," Angewandte Chemie International Edition, vol. 56, no. 46, pp. 14763–14769, Oct. 2017, doi: 10.1002/anie.201708266.

[88] P. Pracht, S. Grimme, C. Bannwarth, F. Bohle, S. Ehlert, G. Feldmann, J. Gorges, M. Müller, T. Neudecker, C. Plett, S. Spicher, P. Steinbach, P.A. Wesołowski, F. Zeller, "CREST—A program for the exploration of low-energy molecular chemical space," The Journal of Chemical Physics, vol. 160, no. 11, Mar. 2024, doi: 10.1063/5.0197592.

[89] C. Devereux, J. S. Smith, K. K. Huddleston, K. Barros, R. Zubatyuk, O. Isayev, and A. E. Roitberg, "Extending the Applicability of the ANI Deep Learning Molecular Potential to Sulfur and Halogens," Journal of Chemical Theory and Computation, vol. 16, pp. 4192–4202, Jun. 2020, doi: 10.1021/acs.jctc.0c00121.

[90] D. M. Anstine, R. Zubatyuk, and O. Isayev, "AIMNet2: a neural network potential to meet your neutral, charged, organic, and elemental-organic needs," Chemical Science, vol. 16, pp. 10228–10244, 2025, doi: 10.1039/D4SC08572H.

[91] D. P. Kovács, J. H. Moore, N. J. Browning, I. Batatia, J. T. Horton, Y. Pu, V. Kapil, W. C. Witt, I.-B. Magdău, D. J. Cole, and G. Csányi, "MACE-OFF: Short-Range Transferable Machine Learning Force Fields for Organic Molecules," Journal of the American Chemical Society, vol. 147, pp. 17598–17611, May 2025, doi: 10.1021/jacs.4c07099.

[92] Y. Guan, S. V. S. Sowndarya, L. C. Gallegos, P. C. St. John, and R. S. Paton, "Real-time prediction of 1H and 13C chemical shifts with DFT accuracy using a 3D graph neural network," Chemical Science, vol. 12, pp. 12012–12026, 2021, doi: 10.1039/D1SC03343C.

[93] A. Howarth, K. Ermanis, and J. M. Goodman, "DP4-AI automated NMR data analysis: straight from spectrometer to structure," Chemical Science, vol. 11, pp. 4351–4359, 2020, doi: 10.1039/D0SC00442A.

[94] B. Jing, G. Corso, J. Chang, R. Barzilay, and T. Jaakkola, "Torsional Diffusion for Molecular Conformer Generation," Advances in Neural Information Processing Systems 35 (NeurIPS 2022), 2022, arXiv:2206.01729.

[95] O.-E. Ganea, L. Pattanaik, C. W. Coley, R. Barzilay, K. F. Jensen, W. H. Green, and T. S. Jaakkola, "GeoMol: Torsional Geometric Generation of Molecular 3D Conformer Ensembles,"

Advances in Neural Information Processing Systems 34 (NeurIPS 2021), 2021, arXiv:2106.07802.

[96] A.S. Perera, C.D. Carlson, J. Cheramy, Y. Xu, Citing, "Infrared and vibrational circular dichroism spectra of methyl β-D-glucopyranose in water: The application of the quantum cluster growth and clusters-in-a-liquid solvation models," Chirality, vol. 35, no. 10, pp. 718–731, May 2023, doi: 10.1002/chir.235

[97] P. Hamm, M. Zanni,"Concepts and Methods of 2D Infrared Spectroscopy," Vol. 1. Cambridge: Cambridge University Press, 2011.

[98] W. Wang and V. Deckert, "Tip-Enhanced Raman Spectroscopy," Raman Spectroscopy, pp. 233–289, 2024, doi: 10.1007/978-981-97-1703-3_11.

[99] R. Franco, S. Gil-Caballero, I. Ayala, A. Favier, and B. Brutscher, "Probing Conformational Exchange Dynamics in a Short-Lived Protein Folding Intermediate by Real-Time Relaxation–Dispersion NMR," Journal of the American Chemical Society, vol. 139, no. 3, pp. 1065–1068, Jan. 2017, doi: 10.1021/jacs.6b12089.

[100] M.-K. Lee, M. Gal, L. Frydman, and G. Varani, "Real-time multidimensional NMR follows RNA folding with second resolution," Proceedings of the National Academy of Sciences, vol. 107, no. 20, pp. 9192–9197, May 2010, doi: 10.1073/pnas.1001195107.

[101] V. Kumar, "In-cell NMR spectroscopy: A tool to study cellular structure biology," Advances in Protein Molecular and Structural Biology Methods, pp. 267–276, 2022, doi: 10.1016/b978-0-323-90264-9.00017-9.

[102] S. Basak and K. Chattopadhyay, "Studies of protein folding and dynamics using single molecule fluorescence spectroscopy," Physical Chemistry Chemical Physics, vol. 16, no. 23, p. 11139, 2014, doi: 10.1039/c3cp55219e.

[103] P. S. Kumagai, A. P. U. Araujo, and J. L. S. Lopes, "Going deep into protein secondary structure with synchrotron radiation circular dichroism spectroscopy," Biophysical Reviews, vol. 9, no. 5, pp. 517–527, Aug. 2017, doi: 10.1007/s12551-017-0314-2.

[104] A. A. Altaf, S. Kausar, and A. Badshah, "Spectral Calculations with DFT," Density Functional Calculations - Recent Progresses of Theory and Application, May 2018, doi: 10.5772/intechopen.71080.

[105] E.B. Wilson, J.C. Decius, P.C. Cross, "Molecular Vibrations: The Theory of Infrared and Raman Vibrational Spectra," Vol. 102. New York: McGraw-Hill, 1955.

[106] M. H. Jamróz, "Vibrational Energy Distribution Analysis (VEDA): Scopes and limitations," Spectrochimica Acta Part A: Molecular and Biomolecular Spectroscopy, vol. 114, pp. 220–230, Oct. 2013, doi: 10.1016/j.saa.2013.05.096.

[107] T. A. Mohamed, G. A. Guirgis, Y. E. Nashed, and J. R. Durig, "Spectra and structure of silicon containing compounds," Vibrational Spectroscopy, vol. 30, no. 2, pp. 111–120, Nov. 2002, doi: 10.1016/s0924-2031(02)00003-6.

[108] I. A. Shaaban, M. A. Assiri, T. E. Ali, and T. A. Mohamed, "Keto-enol tautomerism, spectral (infrared, Raman and NMR) studies and Normal coordinate analysis of 4-Methyl-2-hydroxyquinoline using quantum mechanical calculations," Journal of Molecular Structure, vol. 1252, p. 132137, Mar. 2022, doi: 10.1016/j.molstruc.2021.132137.

[109] C. Cuadrado, F. Cen-Pacheco, and A. H. Daranas, "Computationally Assisted Analysis of NMR Chemical Shifts as a Tool in Conformational Analysis," Organic Letters, vol. 26, no. 31, pp. 6529–6534, Jun. 2024, doi: 10.1021/acs.orglett.4c01642.

[110] J. Li, J. Liang, Z. Wang, A.L. Ptaszek, X. Liu, B. Ganoe, M. Head-Gordon, T. Head-Gordon, "Highly Accurate Prediction of NMR Chemical Shifts from Low-Level Quantum Mechanics Calculations Using Machine Learning," Journal of Chemical Theory and Computation, vol. 20, no. 5, pp. 2152–2166, Feb. 2024, doi: 10.1021/acs.jctc.3c01256.

[111] G. Saielli, K. C. Nicolaou, A. Ortiz, H. Zhang, and A. Bagno, "Addressing the Stereochemistry of Complex Organic Molecules by Density Functional Theory-NMR: Vannusal B in Retrospective," Journal of the American Chemical Society, vol. 133, no. 15, pp. 6072–6077, Mar. 2011, doi: 10.1021/ja201108a.

[112] A. C. F. de Albuquerque, L. H. Martorano, and F. M. dos Santos, "Are we still chasing molecules that were never there, The role of quantum chemical simulations of NMR parameters in structural reassignment of natural products," Frontiers in Natural Products, vol. 2, Jan. 2024, doi: 10.3389/fntpr.2023.1321043.

[113] H. Shi, I.N. Michaelides, B. Darses, P. Jakubec, Q.N.N. Nguyen, R.S. Paton, D.J. Dixon, "Total Synthesis of (−)-Himalensine A," Journal of the American Chemical Society, vol. 139, no. 49, pp. 17755–17758, Nov. 2017, doi: 10.1021/jacs.7b10956.

[114] Q.N.N. Nguyen, J. Schwochert, D.J. Tantillo, R.S. Lokey ,"Using ^{1}H and ^{13}C NMR chemical shifts to determine cyclic peptide conformations: a combined molecular dynamics and quantum mechanics approach," Physical Chemistry Chemical Physics, vol. 20, no. 20, pp. 14003–14012, 2018, doi: 10.1039/c8cp01616j.

[115] J. K. Sader and J. E. Wulff, "Reinvestigation of a robotically revealed reaction," Nature, vol. 570, no. 7762, pp. E54–E59, Jun. 2019, doi: 10.1038/s41586-019-1176-5.

[116] S.-M. Shen, G. Appendino, and Y.-W. Guo, "Pitfalls in the structural elucidation of small molecules. A critical analysis of a decade of structural misassignments of marine natural products," Natural Product Reports, vol. 39, no. 9, pp. 1803–1832, 2022, doi: 10.1039/d2np00023g.

[117] F. Wang, "Future of computational molecular spectroscopy—from supporting interpretation to leading the innovation," Physical Chemistry Chemical Physics, vol. 25, no. 10, pp. 7090–7105, 2023, doi: 10.1039/d3cp00192j.

[118] J.J. La Clair,"Total Syntheses of Hexacyclinol, 5-epi-Hexacyclinol, and Desoxohexacyclinol Unveil an Antimalarial Prodrug Motif," Angewandte Chemie, vol. 118, no. 17, pp. 2835–2839, Apr. 2006, doi: 10.1002/ange.200504033.

[119] S. D. Rychnovsky, "Predicting NMR Spectra by Computational Methods: Structure Revision of Hexacyclinol," Organic Letters, vol. 8, no. 13, pp. 2895–2898, Jun. 2006, doi: 10.1021/ol0611346.

[120] J. A. Porco, S. Su, X. Lei, S. Bardhan, and S. D. Rychnovsky, "Total Synthesis and Structure Assignment of (+)-Hexacyclinol," Angewandte Chemie International Edition, vol. 45, no. 35, pp. 5790–5792, Aug. 2006, doi: 10.1002/anie.200602854.

[121] I. Cortés, C. Cuadrado, A. Hernández Daranas, and A. M. Sarotti, "Machine learning in computational NMR-aided structural elucidation," Frontiers in Natural Products, vol. 2, Jan. 2023, doi: 10.3389/fntpr.2023.1122426.

[122] J. F. Stanton and R. J. Bartlett, "The equation of motion coupled-cluster method. A systematic biorthogonal approach to molecular excitation energies, transition probabilities, and excited state properties," The Journal of Chemical Physics, vol. 98, no. 9, pp. 7029–7039, May 1993, doi: 10.1063/1.464746.

[123] A. G. Petrovic, N. Berova, and J. L. Alonso-Gómez, "Absolute Configuration and Conformational Analysis of Chiral Compounds via Experimental and Theoretical Prediction of Chiroptical Properties: ORD, ECD, and VCD," Structure Elucidation in Organic Chemistry, pp. 65–104, Dec. 2014, doi: 10.1002/9783527664610.ch3.

[124] S. Superchi, P. Scafato, M. Gorecki, and G. Pescitelli, "Absolute Configuration Determination by Quantum Mechanical Calculation of Chiroptical Spectra: Basics and Applications to Fungal Metabolites," Current Medicinal Chemistry, vol. 25, no. 2, pp. 287–320, Jan. 2018, doi: 10.2174/0929867324666170310112009.

[125] M. V. Cooke, I. Malvacio, W. J. Peláez, A. J. Pepino, M. R. Mazzieri, and G. A. Argüello, "TD-DFT calculations of UV absorption bands and their intensities in the spectra of some tetrahydroquinolines," RSC Advances, vol. 5, no. 33, pp. 26255–26262, 2015, doi: 10.1039/c5ra00249d.

[126] Y. Morisawa, Y. Higaki, and Y. Ozaki, "Far-Ultraviolet Spectroscopy and Quantum Chemical Calculation Studies of the Conformational Dependence on the Electronic Structure and Transitions of Cyclohexane, Methyl and Dimethyl Cyclohexane, and Decalin; Effects of Axial Substitutions on the Electronic Transitions," The Journal of Physical Chemistry A, vol. 125, no. 37, pp. 8205–8214, Sep. 2021, doi: 10.1021/acs.jpca.1c05688.

[127] M. A. Muñoz, "Chiral Chromatographic Analysis and Absolute Stereochemistry of Racemic Chlorpheneramine Using Chiral HPLC-Cd-or and TD-DFT Calculations," Journal of the Chilean Chemical Society, vol. 63, no. 3, pp. 4155–4158, 2018, doi: 10.4067/s0717-9707201800030 4155.

[128] Y. Wang, J. Fleischhauer, S. Bausch, M. Sebestian, and P. H. Laur, "Conformational Analysis and TDDFT Calculations of the Chiroptical Properties of Tris[1,2-propanediolato(2-)-κ O ,κ O ′]-selenium/tellurium and Related Compounds," Enantiomer, vol. 7, no. 6, pp. 343–374, Nov. 2002, doi: 10.1080/10242430215700.

[129] J. Stocka, R. Platakyte, T.M.C. McFadden, J. Ceponkus, V. Aleksa, A.G. Hanna, V. Sablinskas, P. Rodziewicz, G.A. Guirgis , "Conformational diversity of 1-chloro-1-chloromethylsila cyclohexane with experimental (Raman and IR) and computational (DFT, MP2) methods," Journal of Molecular Structure, vol. 1249, p. 131644, Feb. 2022, doi: 10.1016/j.molstruc. 2021.131644.

[130] I. S. Hernandes, H. C. Da Silva, H. F. Dos Santos, and W. B. De Almeida, "Unveiling the Molecular Structure of Antimalarial Drugs Chloroquine and Hydroxychloroquine in Solution through Analysis of ^{1}H NMR Chemical Shifts," The Journal of Physical Chemistry B, vol. 125, no. 13, pp. 3321–3342, Mar. 2021, doi: 10.1021/acs.jpcb.1c00609.

[131] L.-Y. Liu, H. Sun, C. Griesinger, and J.-K. Liu, "The Use of a Combination of RDC and Chiroptical Spectroscopy for Determination of the Absolute Configuration of Fusariumin A from the Fungus Fusarium sp.," Natural Products and Bioprospecting, vol. 6, no. 1, pp. 41–48, Jan. 2016, doi: 10.1007/s13659-015-0084-0.

[132] L. Grauso, R. Teta, G. Esposito, M. Menna, and A. Mangoni, "Computational prediction of chiroptical properties in structure elucidation of natural products," Natural Product Reports, vol. 36, no. 7, pp. 1005–1030, 2019, doi: 10.1039/c9np00018f.

[133] N. Grimblat, M. M. Zanardi, and A. M. Sarotti, "Beyond DP4: an Improved Probability for the Stereochemical Assignment of Isomeric Compounds using Quantum Chemical Calculations of

NMR Shifts," The Journal of Organic Chemistry, vol. 80, no. 24, pp. 12526–12534, Dec. 2015, doi: 10.1021/acs.joc.5b02396.

[134] P. H. Willoughby, M. J. Jansma, and T. R. Hoye, "A guide to small-molecule structure assignment through computation of (1H and 13C) NMR chemical shifts," Nature Protocols, vol. 9, no. 3, pp. 643–660, Mar. 2014, doi: 10.1038/nprot.2014.042.

[135] A. V. Marenich, S. V. Jerome, C. J. Cramer, and D. G. Truhlar, "Charge Model 5: An Extension of Hirshfeld Population Analysis for the Accurate Description of Molecular Interactions in Gaseous and Condensed Phases," Journal of Chemical Theory and Computation , vol. 8, no. 2, pp. 527–541, Jan. 2012, doi: 10.1021/ct200866d.

[136] Y. Hu, P. Ounkham, O. Marsalek, T. E. Markland, B. Krishmoorthy, and A. E. Clark, "Persistent Homology Metrics Reveal Quantum Fluctuations and Reactive Atoms in Path Integral Dynamics," Frontiers in Chemistry, vol. 9, Mar. 2021, doi: 10.3389/fchem.2021.624937.

[137] J. Liu, L.-W. Qi, J. Z. H. Zhang, and X. He, "Fragment Quantum Mechanical Method for Large-Sized Ion–Water Clusters," Journal of Chemical Theory and Computation, vol. 13, no. 5, pp. 2021–2034, Apr. 2017, doi: 10.1021/acs.jctc.7b00149.